U.S. DEPARTMENT OF COMMERCE
National Oceanic and Atmospheric Administration
Environmental Research Laboratories

NOAA Technical Memorandum ERL NSSL-62

MESOSCALE OBJECTIVE MAP ANALYSIS USING WEIGHTED TIME-SERIES OBSERVATIONS

Stanley L. Barnes

Property of
NWC Library
University of Oklahoma

National Severe Storms Laboratory
Norman, Oklahoma
March 1973

TABLE OF CONTENTS

LIST OF FIGURES

LIST OF TABLES

ABSTRACT

An objective map analysis technique applicable to quasi-steady, translating atmospheric circulations is developed from the mathematical premise that distributions of meteorological variables can be represented by an infinite sum of independent, harmonic waves. In addition to the usual space-weighting of simultaneous observations to obtain interpolated values at regularly arrayed grid points, the scheme uses asynoptic observations by positioning them relative to a moving disturbance and weighing them according to both space and time.

Arbitrary weight function parameters provide analyses for specific needs: they depict only long wave components or extract whatever detail is represented in the data set. The rate at which an analysis converges to fit observations is controllable--required details can be resolved in only one iteration of the technique.

Analysis response for several choices of the arbitrary parameters is tested on simple analytically determined distributions and on selected meteorological observations during the passage of three thunderstorms over the National Severe Storms Laboratory mesonetwork of surface and upper air stations in central Oklahoma. Incorporating time series observations improves the analysis of those disturbances that are large enough to be sensed unambiguously by the station network. However, basic resolution capability is governed more by the spatial density of observations as opposed to frequency of observations. The analyses are not particularly sensitive to small uncertainties (or real variations) in the disturbance translation velocity.

Upper air analyses tested for along-the-wind (elliptic) enhancement of the weight function are insensitive to this enhancement except when actual wind speeds exceed the "characteristic" speed by a factor of two or more, but then analyses deteriorate.

MESOSCALE OBJECTIVE MAP ANALYSIS USING WEIGHTED TIME-SERIES OBSERVATIONS

Stanley L. Barnes
National Severe Storms Laboratory

1. INTRODUCTION

The basis of this objective map analysis was developed in an earlier paper (Barnes, 1964) upon a suggestion by Sasaki (1960). The scheme, similar in some respects to the Cressman method (1959), uses weighted averages of observed data to determine two-dimensional distributions of interpolated values at grid points of a square mesh. In the previous application, the distance-dependent weight factor could be selected judiciously to maximize details supportable by the observation density and representativeness. The interpolated field was made to converge to observed values by adding weighted correction fields in an iterative fashion. The attained convergence was a function of wavelength (or the characteristic distance between extrema) and the number of iterations.

Two recent modifications of this objective analysis method have been developed: the first reduces to one the iterations required to obtain the desired fit of interpolated field to observations; the second enhances detail in the interpolated field by incorporating time-series observations (either regular or irregular time intervals).

Both modifications have grown of necessity in developing computer analyses applicable to mesonetwork surface and upper air data of the National Severe Storms Laboratory (NSSL). The extraordinary number of surface observations obtained in only one thunderstorm required inordinately long computer time to derive small-scale details supportable by this high resolution data. However, by changing a weight function parameter, details heretofore requiring four or more passes through the data became discernible only with two passes (one iteration). The first portion of this paper describes the modification details and discusses a technique for choosing the initial weight function parameter to obtain desired pattern detail.

Although the NSSL upper air rawinsonde networks have been densely instrumented in keeping with the scale of the phenomenon under study, relatively large data gaps in time and space still exist in individual storms. Balloons released at irregular intervals from various sites seldom reach given altitudes at the same time; furthermore, they are displaced horizontally according to the vagaries of the wind fields through which they rise. Also it's imperative to consider the positions of these observations relative to the moving storms. Clearly, a useful analysis technique would accommodate these uncontrollable variations in data acquisition.

Several authors have proposed methods to incorporate past data into dynamical analysis-prediction schemes (e.g., Miyakoda and Talagrand, 1971). These methods usually involve positioning past observations according to some prediction scheme and mixing these data with current data, either on

an equivalent basis or weighted according to the data's age. Optimal interpolation methods are used to minimize the variance between observed and predicted values.

In the study of mesoscale circulations, large severe thunderstorms in particular, dynamical prediction of essential three-dimensional atmospheric properties has not been accomplished yet with adequate skill. Indeed, many important thunderstorm characteristics have not been adequately described (or even observed). We face the task of developing a method that will reveal these details (hopefully) or indicate the nature of required additional observations. The method presented here provides a "first look" at the three-dimensional structure of the atmosphere; horizontal distributions are analyzed at selected levels without constraints on the vertical distributions. Sophisticated, dynamically-constrained analyses may be required before a more complete picture of thunderstorm mechanics emerges.

Since severe thunderstorms tend to be large (20 to 50 km) and long lived (several hours), analysis by time-to-space conversion has been used frequently assuming the data relevant to a quasi-steady, moving system (Fujita, 1963). Typically, time series observations at individual stations (of temperature, for example) are manually plotted according to the translation velocity of the phenomenon being analyzed. Each observation, once positioned in space, is subjectively evaluated to determine the (temperature) distribution. Generally the analyst does not accommodate all the data, but consciously smooths the distribution according to some concept of the observed phenomenon's relevant pattern. Influence assigned to "off-time" observations is often a function of data density. When positioned among observations not well correlated, usually the "off-time" observation is suppressed or "averaged" with the other observations. However, when occurring by itself, the off-time observation frequent is assigned a high influence simply because there are no other reports to weigl

In this computer technique, time series observations are treated in much the same fashion. First, observations are positioned relative to a moving storm. Then weight is assigned objectively to each observation according to its age. Density of observations still has an important influence on the interpolated values at grid points, but if several observations are equidistant from a grid point, those nearer to map time carry the greater weight at that point.

Although the objective time-to-space analysis technique was designed especially for application to sounding data, it has been highly useful in analyzing the more densely instrumented surface network data. In the following sections are technical details for applying this scheme, a discussion of tests which guide the choice of arbitrary parameters, and typical results.

2. SPACE RESPONSE FUNCTION

For clarity in discussing the time weighting technique, we derive in detail the response function summarized in an earlier paper (Barnes, 1964).

Suppose an atmospheric variable distributes as $f(x,y) = A \sin ax$ which is uniform in y-direction for simplicity. Assume a continuum of obser-

vations regarding f(x,y), and filter (weigh) these data according to their distance from an arbitrary point (x,y). That is,

$$g(x,y) = \int_0^{2\pi} \int_0^{\infty} f(x+r\cos\theta,\ y+r\sin\theta)\ w(r,k)\ r\ dr\ d\theta \qquad (1)$$

where r is shown in figure 1, and the weight function is

$$w(r,k) = [1/4\pi k]\ \exp(-r^2/4k); \qquad (2)$$

k is an arbitrary parameter. We wish to determine the relationship between observed value, f, and weighted average value, g, at the same point (x,y).

$$g(x,y) = D(a,k)\ f(x,y). \qquad (3)$$

D(a,k) is the response function and is wavelength dependent (wave number $a = \pi/L$, where L is half the wavelength).

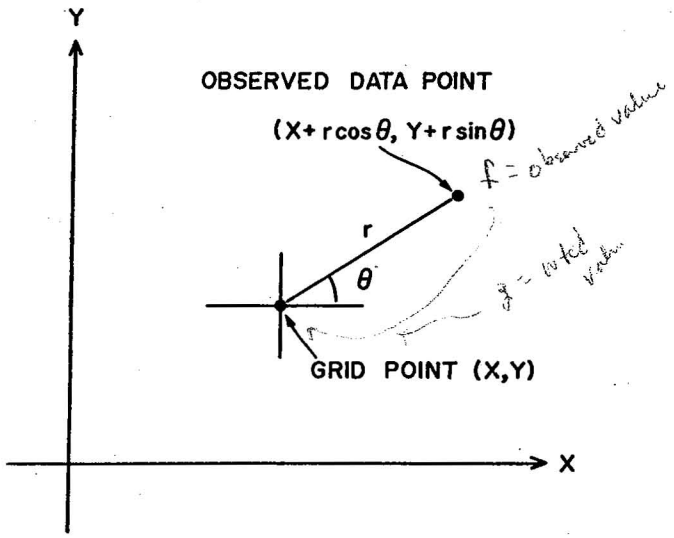

Figure 1. Coordinate system used in objective analysis expressed by (1). Point (x,y) is conveniently chosen as a grid point of a square mesh; point (x + rcosθ, y + rsinθ) represents one point where information is observed. Theoretically, these are continuously arrayed over the x-y plane, but in the practical application, they are discrete points, irregularly arrayed.

Consider

$$f(x+r\cos\theta,\ y+r\sin\theta) = A\ \sin[a(x+r\cos\theta)] \tag{4}$$

$$= A\ \sin(ax)\ \cos[a(r\cos\theta)] + A\ \cos(ax)\ \sin[a(r\cos\theta)].$$

Substituting (2) and (4) into (1),

$$g(x,y) = A\ \sin(ax)\int_0^{2\pi}\int_0^{\infty} \cos[a(r\cos\theta)](1/4\pi k)\exp(-r^2/4k)r\,dr\,d\theta \tag{5}$$

$$+ A\ \cos(ax)\int_0^{2\pi}\int_0^{\infty} \sin[a(r\cos\theta)]\ (1/4\pi k)\exp(-r^2/4k)r\,dr\,d\theta.$$

Considering only the integral with respect to θ in the first term, we note that it is an integral form of zero order Bessel function (see Abramowitz and Stegun, 1965; page 360, Eq. 9.1.18):

$$\int_0^{2\pi} \cos[a(r\cos\theta)]d\theta = 2\int_0^{\pi} \cos[a(r\cos\theta)]d\theta = 2\pi\ J_0(ar). \tag{6}$$

The second term of (5) vanishes for the following reason (page 361, Eq. 9.1.45 of Abramowitz and Stegun, 1965):

$$\int_0^{2\pi} \sin[a(r\cos\theta)]d\theta = 2\sum_{k=0}^{\infty} (-1)^k\ J_{2k+1}(ar)\int_0^{2\pi} \cos[(2k+1)\theta]d\theta$$

$$= 2\sum_{k=0}^{\infty} (-1)^k\ J_{2k+1}(ar)\ (1/2k+1)\ \sin[(2k+1)\theta]_0^{2\pi} \tag{7}$$

$$= 0$$

since only integer multiples of π appear as sine arguments.

By (6) and (7), (5) becomes

$$g(x,y) = (A/2k)\sin(ax)\int_0^{\infty} J_0(ar)\exp(-r^2/4k)r\,dr. \tag{8}$$

The integral in (8) has the same form as Eq. 11.4.29, page 486 of Abramowitz and Stegun (1965) and meets the conditions for solution expressed therein Thus, the filtered response to f(x,y) is

$$g(x,y) = \exp(-a^2k)\ [A\ \sin(ax)]. \tag{9}$$

Note that the response function

$$D(a,k) = \exp(-a^2k) \tag{10}$$

a = wave number $= \frac{2\pi}{L} = \frac{2\pi}{\lambda}$

here $L = \lambda$

$D = \exp(-a^2 k)$

$-a^2 = -\frac{\pi^2 4}{\lambda^2}$

$a = \frac{2\pi}{\lambda}$

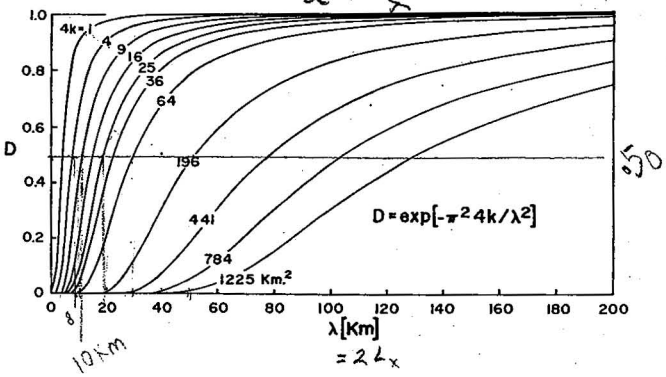

Figure 2. Relationship of response function (10) to wavelength λ for various choices of parameter k. Responses correspond to one pass through the data with filter (2).

λ = wavelength

cannot alter the phase of the original function, but acts only to damp the amplitude. (We discuss in sec. 3 a simple technique for regaining amplitude.) Figure 2 indicates the nature of D(a,k) as a function of wavelength, $\lambda = 2L$, and for various arbitrary choices of parameter k. In general, response is nearly zero for very short waves and approaches one for very long waves. The wavelength range in figure 2 covers the scale of phenomena most interesting to NSSL studies. However, applications of the analysis technique aren't restricted to mesoscale distributions.

We can approximate a more complicated function, f(x,y), as the finite sum of a number of independent waves of type (4) and discuss the properties of D(a,k) that make it a selective filter. As k decreases, the effective cutoff wavelength is more sharply defined. For example, with $4k = 441$ km^2, the range of wavelengths for which the response is between 0.2 and 0.8 is about 88 km. With $4k = 36$ km^2, this range is only 25 km.

Ideally one can choose a small k and yet be confident that extremely small waves ("noise") will be suppressed relatively well. However, the practical lower limit on k is governed by the data distribution. Throughout this discussion, a continuum of information exists concerning f(x,y). In the real world, this is never achieved; the data distribution further degrades the response to the filtering process. If the spacing between data points is 20 km, then it isn't relevant to talk about response to smaller than 40-km waves except as they may appear aliased in longer waves. If the data are not evenly distributed, then phase changes and a higher "noise" level are inherent to the analyzed (interpolated) field; consequently, further restrictions are placed on the smallest meaningful resolvable features. These problems, demonstrated in test results, are discussed later.

Phase is not altered, just amplitude

3. FORCING ANALYSES TO FIT OBSERVED DATA

In the earlier paper describing this analysis technique, a method of successive corrections fits the interpolated function, $g(x,y)$, to the observations within an arbitrarily small difference. Briefly, the technique involved successive applications of the same filter (weight function) to the residual differences between $g(x,y)$ and $f(x,y)$ on each of an arbitrary number of passes through the data. The devised scheme was also mathematically convergent. Its main drawback was the large number of iterations and computer time required to achieve adequate response to short wavelengths.

Since then, a modification has been developed that requires only one correction pass through the data to achieve the desired response at small wavelengths. Decreasing the weight function parameter k on the first correction pass increases the convergence rate to meet arbitrary analysis requirements and saves considerable computation time.

Rewrite (9) and (10) as

$$g_o(x,y) = D_o f(x,y). \tag{11}$$

Subscript zero denotes the first pass result through the data with weight function $\eta_o = \exp(-r^2/4k_o)$. In a manner similar to (13) through (15) of the previous paper, the second pass yields smoothed values of the residual differences between $f(x,y)$ and $g(x,y)$ which are added to the first pass field:

$$g_1(x,y) = g_o(x,y) + [f(x,y) - g_o(x,y)]D_1 \tag{12}$$

where D_1 is the response resulting from application of weight function

$$\eta_1 = \exp(-r^2/4k_1);\ k_1 = \gamma k_o \text{ and } \gamma > 0. \tag{13}$$

Thus,

$$D_1 = \exp(-a^2 k_1) = \exp(-a^2 \gamma k_o) = D_o^{\gamma}. \tag{14}$$

Substituting (14) and (11) into (12), we have

$$g_1(x,y) = f(x,y)\, D_o\, [1 + D_o^{\gamma-1} - D_o^{\gamma}]. \tag{15}$$

The new response function is now

$$D' = D_o(1 + D_o^{\gamma-1} - D_o^{\gamma}) \qquad (16)$$

instead of

$$D' = D_o \sum_{n=0}^{N} (1 - D_o)^n \qquad (17)$$

as derived in the previous paper (Eq. 20).

Compared to the Cressman (1959) method for restoring short waves by successive scans with decreased influence radii, this method has these four advantages.

1. Weight factor 4k can be chosen prior to the analysis so that pattern scales supportable by the data distribution will be revealed, and to a known response amplitude.

2. Because (2) approaches zero asymptotically, the influence of data can be extended any distance without changing the weight function and, therefore, the response characteristics. In the Cressman technique, the weight function shape is tied to an influence radius beyond which zero weight applies. To insure that sufficient data influence the interpolation in data sparse regions, the current scan radius is locally increased in some applications (Inman, 1970) until a minimum number of observations are included. Such a locally varying weight factor produces unknown response in the final result, and introduces small scale irregularities ("noise") which must be smoothed by later application of arbitrary filters.

3. Small scale irregularities are adequately suppressed by this technique so further smoothing by application of additional numerical filters (e.g., Shuman, 1957) is not necessary.

4. The desired pattern resolution can be achieved in only one iteration, instead of four or more required with Cressman's technique, thus effecting a modest savings in computer time.

These advantages are illustrated by test results in appendix A.

Figure 3 is a graph of (16) showing D' versus D_o for various values of γ. Recall that the initial response (given k) is proportional to wavelength (see fig. 2). The line $\gamma = 1.0$ corresponds to the response after one iteration using the old technique (17). The new technique with $\gamma < 1$ recovers short wavelength amplitudes very quickly. Compare the increase in D' at two wavelengths, one that has been represented with initial response $D_o = 0.5$ and one that has initial response $D_o = 0.2$. The result of one

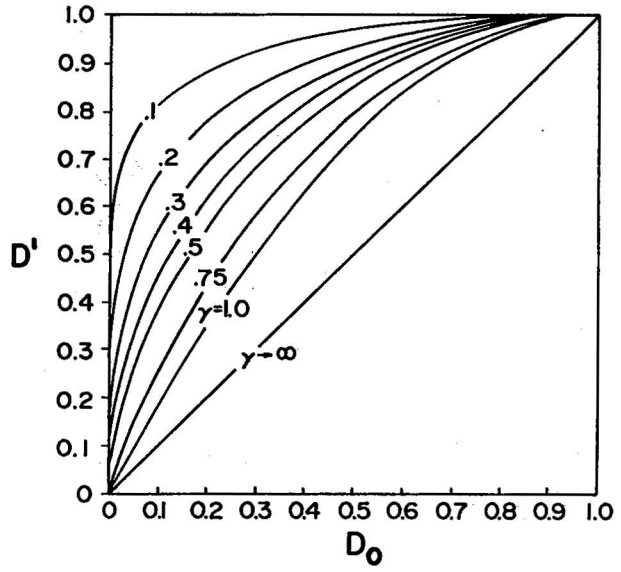

Figure 3. Response D' after one correction pass as a function of initial response D_o and arbitrary parameter γ (see (16)).

iteration using the old method ($\gamma = 1.0$) increases the responses to about 0.75 and 0.36. By the new method with $\gamma = 0.5$, say, the responses will be about 0.85 and 0.56. The short wavelength amplitude gain is 20 percent compared with 10 percent for the long wave. A comparable response using the old method required three iterations (four passes) through the data (see fig. 2, Barnes, 1964). Even greater responses at short wavelengths are obtainable by choosing γ smaller than 0.5, but the wisdom of such a choice depends upon several factors including the purpose of the analysis and the data representativeness. Our experience indicates that γ can't be smaller than about 0.2 without creating underflow checks on most computer systems (i.e., negative arguments of the exponential function too large to evaluate). Also, specifying $\gamma > 0.5$ does not produce rapid analysis convergence. Empirically then, an optimum γ appears to lie in the range 0.2 to 0.4.

With information derived thus far, practical guidelines for choosing k and γ in the spatial weight function can be considered. Suppose observations are available at points more or less evenly distributed and spaced on the order of 20 km. Further suppose that magnitudes of instrumental and data processing uncertainties are small compared with the expected amplitude of atmospheric variations on the same scale (i.e., wavelength 40 km). Require that the analysis depict at least 90 percent amplitude of this smallest resolvable scale of variations. Tentatively let $\gamma = 0.3$. Turn now to figure 4 in which D' is plotted as a function of 4k and λ for $\gamma = 0.3$. The intersection of the curve D' = 0.9 with λ = 40 km occurs near the value $4k = 110$ km^2. Thus, for the prescribed analysis, $4k = 110$ km^2 and $\gamma = 0.3$ should produce the desired response. Choose some other γ, say 0.2 or 0.4, and the same response (D' = 0.9) is achieved with $4k = 145$ km^2 or $4k = 95$ km^2 (dashed curves in fig. 4).

When accuracy or representativeness of data are questionable, it is unwise to force the analysis to represent the smallest scale definable by the data distribution. Rather some filtering of the "noise" is desirable. Had this been the aim in treating the above data set, we might have required the final response at λ = 40 km to be less than 0.5. With $\gamma = 0.3$, $4k = 410$ km^2 (fig. 4) gives the desired result.

Practically, the actual data distribution is by far the most critical factor influencing the analysis. As the density of observations decreases or becomes irregular, results become more sensitive to choices in the weight

parameters.[1]

4. RESPONSE FUNCTIONS FOR STEADILY TRAVELLING WAVES

In the real atmosphere, disturbances invariably move and change character. When a large number of simultaneous observations aren't available for recreating the spatial distribution of a given meteorological variable, then it becomes necessary to use the atmosphere's predictable characteristics to enhance the available information. The manner in which temporal information is put into the analysis is critical. Averaging in time before analyzing spatially produces results which are strongly damped over a wide range of translation velocities common to meteorological disturbances. Another technique, time-to-space conversion, yields results similar to those obtainable with simultaneous observations alone, but with enhanced details--a consequence of an effective increase in observation density. Furthermore, as shown later, pattern details in the latter scheme are relatively insensitive to small variations (uncertainties) in translation speed. The time averaging technique can be treated mathematically, while time-to-space conversion is amenable only to numerical experiments.

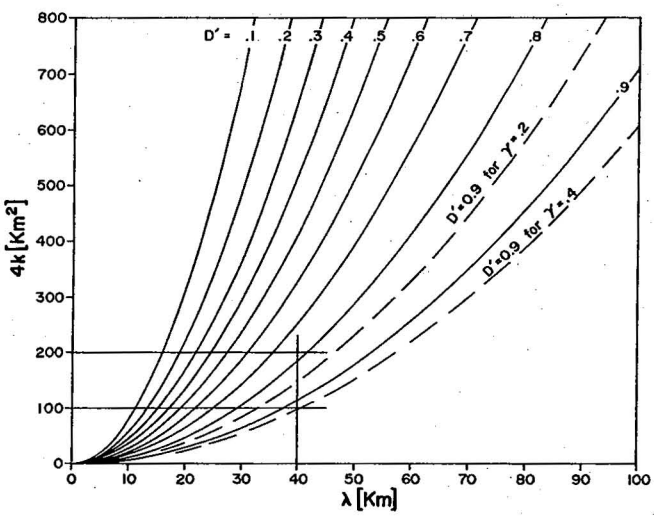

Figure 4. Final response D' as a function of wavelength λ and weight parameter k for $\gamma = 0.3$. For responses with other γ, compare dashed curves to D' = 0.9 curve.

4.1 Response to Time-Averaging Technique

Arithmetic or other weighted averaging of time series data over some arbitrary interval is an effective means of reducing "signal" variance due to high frequency components (Panofsky and Brier, 1958), and a Gaussian weight function (similar in form to (2)) provides better control over aliasing

[1] In the 1964 paper, the weight function $\eta = \exp(-r^2/4k)$ (see fig. 5) was chosen on the basis of an arbitrary relationship $4k = R^2/E$ with E = 4 and R defined as the "radius of influence" beyond which an observation exerted zero influence in determining g(x,y). The tendency was to choose R only slightly larger than the average distance between observations to allow g(x,y) to converge more quickly to f(x,y). However, irregular observation density generates noise in g(x,y) if R happens to be choosen near the dimension of the data gaps. In the current technique, weight function parameter 4k, can be chosen large enough to reduce noise due to variations in observation density because the convergence is controlled by the choice of γ.

problems than does arithmetic ("boxcar") averaging (Muller, 1966). Although the analysis technique described in this section has not been used for assimilation of time series data in an objective map analysis, it may interest the reader to discover the response of time-averaging schemes to travelling waves.

In a manner similar to section 2, consider

$$g(x,y,t) = \int_{-\infty}^{\infty} \int_{0}^{2\pi} \int_{0}^{\infty} f[x+r\cos\theta - c(t+t'),\ y+r\sin\theta]\,w r\,dr\,d\theta\,dt' \quad (18)$$

where x is in the direction of wave motion, c is phase speed, t is some reference time, and t' is time difference from reference time. For convenienc we define

$$w(r,t) = [1/(8\pi^{3/2}k\nu^{1/2})]\exp(-r^2/4k - t'^2/4\nu). \quad (19)$$

Figure 5 indicates the weight function shape as it relates to k and ν .

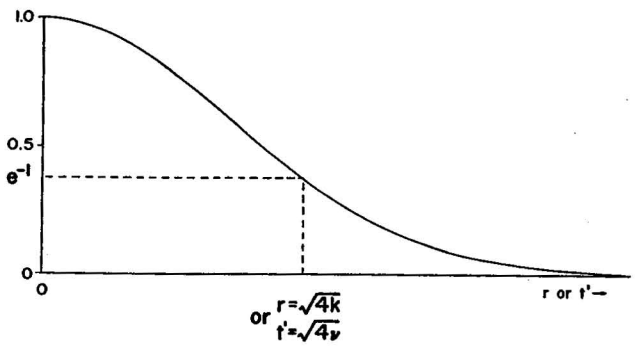

Figure 5. Exponential weight function for space and time analysis ((19) with coefficient suppressed). Abscissa is either radial distance from observation to grid point (see fig. 1) or time difference from reference map time. Shape of weight curve is determined by choice of arbitrary parameters k or ν .

The coefficient in (19) stems from the requirement that

$$\int_{-\infty}^{\infty} \int_{0}^{2\pi} \int_{0}^{\infty} w r\,dr\,d\theta\,dt' = 1. \quad (20)$$

Consider a single translating wave train:

$$f(x+r\cos\theta - c(t+t'),\ y+r\sin\theta) = A\sin[a(x+r\cos\theta - c(t+t'))]. \quad (21)$$

Expanding by the trigonometric relations for angle sums, (21) becomes

$$f = A\sin(ax)\left[\cos[a(r\cos\theta)][\cos(act)\cos(act') - \sin(act)\sin(act')]\right.$$
$$\left. + \sin[a(r\cos\theta)][\sin(act)\cos(act') + \cos(act)\sin(act')]\right]$$
$$+ A\cos(ax)\left[\sin[a(r\cos\theta)][\cos(act)\cos(act') - \sin(act)\sin(act')]\right.$$
$$\left. - \cos[a(r\cos\theta)][\sin(act)\cos(act') + \cos(act)\sin(act')]\right]. \tag{22}$$

Substituting (22) into (18) and considering individual integrals, we note that terms involving sin a(rcosθ) vanish by virtue of (7). Also,

$$\int_{-\infty}^{\infty} \sin(act') \exp(-t'^2/4\nu)\, dt = 0. \tag{23}$$

Proof:

$$\phi(b) = \int_{-\infty}^{\infty} \exp(-\alpha^2 t^2) \sin(bt) dt \tag{24}$$

where $\alpha^2 = 1/4\ \nu$, b = ac (the prime notation on t has been dropped temporarily). Differentiating,

$$\phi' \equiv \frac{d\phi}{db} = \int_{-\infty}^{\infty} t \exp(\alpha^2 t^2) \cos(bt) dt. \tag{25}$$

Integrating by parts with

$$\begin{aligned} u &= \cos(bt) \\ du &= -b \sin(bt)dt \\ dv &= t \exp(-\alpha^2 t^2)dt \\ v &= -(1/2\alpha^2) \exp(-\alpha^2 t^2), \end{aligned} \tag{26}$$

we have

$$\begin{aligned} \phi' = & -(1/2\alpha^2) \exp(-\alpha^2 t^2) \cos(bt) \Big|_{t=-\infty}^{t=\infty} \\ & - (b/2\alpha^2) \int_{-\infty}^{\infty} \exp(-\alpha^2 t^2) \sin(bt) dt. \end{aligned} \tag{27}$$

The first term vanishes in the limit, and we are left with the ordinary differential equation

$$\underline{\phi' = -(b/2\alpha^2)\phi.} \tag{28}$$

The general solution of (28) is

$$\phi = C \exp(-b^2/4\alpha^2). \tag{29}$$

To evaluate C, we note the particular solution

$$\phi(0) = \int_{-\infty}^{\infty} \exp(-\alpha^2 t^2) \sin(bt)dt = 0 \tag{30}$$

for all possible values of t. Thus, ϕ (b) = 0, (23) is proved, and (18) simplifies to

(31)

$$g(x,y,t) = A\sin[a(x-ct)] \int_{-\infty}^{\infty} \int_0^{2\pi} \int_0^{\infty} \cos[a(r\cos\theta)]\cos(act')wrdrd\theta dt'.$$

By virtue of (6) and (19),

$$g(x,y,t) = \frac{A\sin[a(x-ct)]}{4k(\pi\nu)^{1/2}} \int_0^{\infty} J_0(ar) \exp(-r^2/4k)rdr \tag{32}$$

$$\cdot \int_{-\infty}^{\infty} \cos(act') \exp(-t'^2/4\nu)dt.$$

The first integral is the same one that appeared in (8) and has a solution

$$\int_0^{\infty} J_0(ar)\exp(-r^2/4k)rdr = 2k \exp(-a^2k). \tag{33}$$

The second integral is solved by the same technique used to solve (24). The result is

$$\int_{-\infty}^{\infty} \cos(act')\exp(-t'^2/4\nu)dt = 2(\pi\nu)^{1/2} \exp(-a^2c^2\nu). \tag{34}$$

Thus,

$$g(x,y,t) = \exp[-a^2(k + c^2\nu)]A\sin[a(x-ct)]. \tag{35}$$

This response function for time-weighted data applied at the point of observation may be written

$$D_0^* = \exp[-(\pi^2/\lambda^2)(4k + c^2\, 4\nu)] \tag{36}$$

where $\lambda = 2L$ is wavelength.

The sense of this result was anticipated. Short, fast-moving waves are damped while the response to long, slow-moving waves approaches one. However, the response is quite sensitive to variations in ν because it appears in a product with the square of phase speed c. Consider, for example, these parameters in relationship to typical mesoscale phenomena as resolved by the NSSL surface network of autographic recorders. Spacing of observations is about 10 km and typical phase speeds are on the order of 20 kt (0.62 km min^{-1}). The response of analysis scheme (18) and (19) for various wavelengths is shown in figure 6. Parameter 4k has been set equal to 64 km^2. The line $4\nu = 0$ shows the response corresponding to analysis of reference time observations only. This line is identical to the curve labeled 64 in figure 2. Time averaging by weighting according to $\exp(-t'^2/4\nu)$ and applying the weighted values at the observation site always result in some damping of even the longer wave components. Weighting observations $\pm$ 5 min from reference time by e^{-1} ($4\nu = 25$ min^2) further diminishes the analyzed amplitude of 40-km waves by 4 percent, while similar weighting of $\pm$ 10 min data ($4\nu = 100$ min^2) reduces the response by nearly 15 percent. The faster the phase speed, the more drastically reduced is the response. Figure 7 shows a similar set of curves with c = 40 kt (1.24 km min^{-1}). The decreases in response for the above examples are now 14 percent for $4\nu = 25$ min^2 and 40 percent for $4\nu = 100$ min^2.

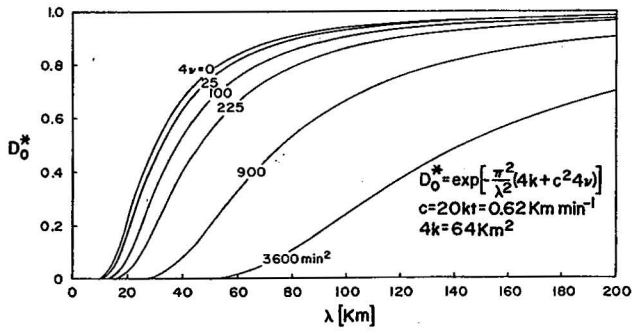

Figure 6. Response function (36) for time-averaging technique applied to simple harmonic wave translating at 20 kt. Because time averaged values are evaluated at point of observation (see fig. 10), this technique suppresses short, fast waves with remarkable efficiency.

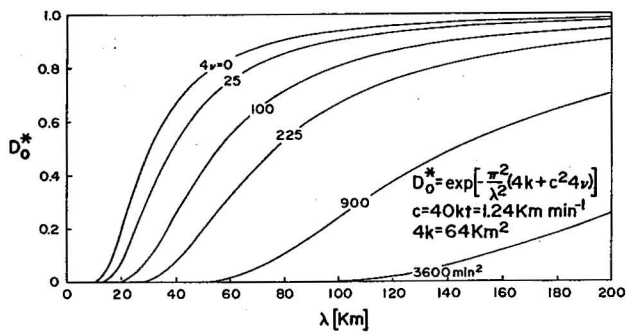

Figure 7. Same as figure 6 except translation speed is doubled to 40 kt.

For observations near reference time ($t' << \sqrt{4\nu}$ in fig. 5), the technique approximates arithmetic averaging of time series data. Clearly, a spatial analysis of such data also yields results significantly damped at small wavelengths.

The responses described here are strictly applicable only when a continuum of observations exists in time. Response influences due to instrumental characteristics and discrete sampling have not been considered, but both are possible sources of noise which should be considered individually.

4.2 Response of Time-To-Space Conversion Technique

The weight function for time-to-space treatment of data has the same form as (19), but the interpretation is not the same. Time difference, t', from reference time applies two ways. First, it determines position of the observation relative to the moving storm such that $\hat{r}' = \hat{c}t'$ where $\hat{c}$ is storm velocity and $\hat{r}'$ is position vector from the station to the displaced observation (fig. 8). Thus, $\hat{r}'$ and $\hat{r}''$, the position vector from grid point to station, added give position vector $\hat{r}$ for the off-time observation relative to a grid point (compare fig. 8 with fig. 1). Second, t' determines the weight (as in fig. 5) assigned to observations according to their age relative to the arbitrary reference time. Parameter ν has this significance: large ν is used for essentially steady systems (all data apply with nearly equal weight regardless when observed); small ν is properly assigned when the phenomenon is changing rapidly relative to the time interval between observations.

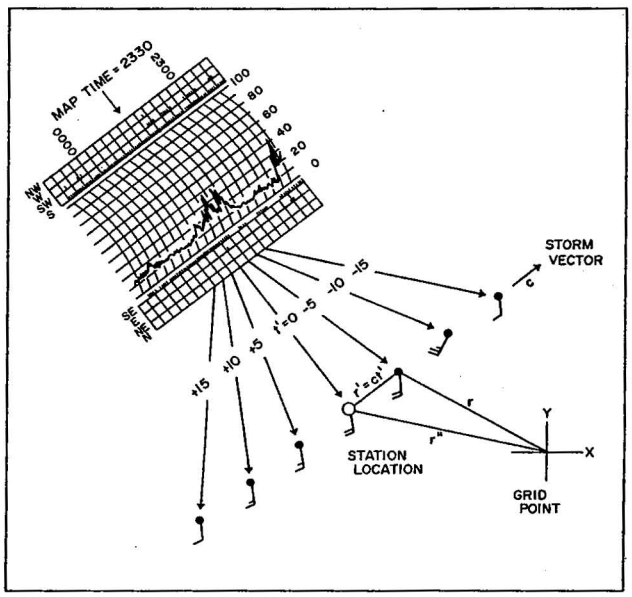

Figure 8. Schematic of time-to-space objective analysis technique illustrated for surface wind observations at 5-min intervals. Station has fixed location, $\hat{r}''$, relative to the example grid point at (x,y). Map time observation is positioned at station and influences interpolated value at grid point in proportion to r''^2. Off-time observations are displaced along storm translation vector, $\hat{c}$, by an amount $\hat{r}' = \hat{c}t'$ and influence grid point value in proportion to r^2 and t'^2 (see (19)).

The response function for this analysis scheme is similar to that for the space weighting scheme in section 2. For steady-state, translating waves, the response is identical to space response function (10). However, if amplitude or phase velocity vary with time, the response will be different from (10) in a manner not easily determined by analytical methods. Note the intractability of (21) and (18) if A and c are even linear time-dependent functions. Therefore, we cannot determine a general response for the time-to-space weighting technique, but we can demonstrate that response to a steady, translating wave is equivalent to the space weighting response.

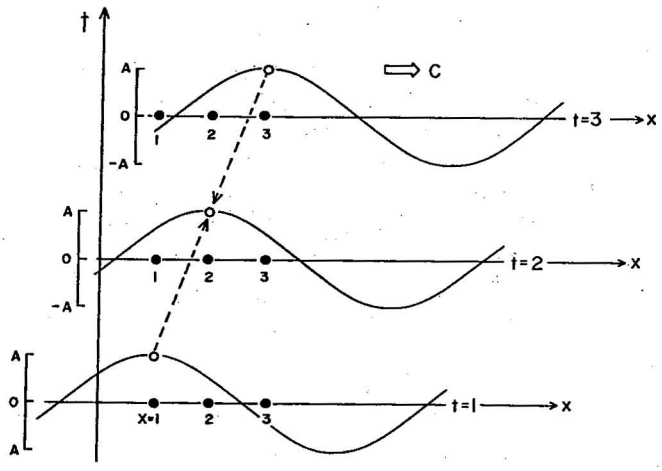

Figure 9. Steadily translating, one-dimensional wave train observed at stations located at solid dots. Time-to-space conversion of sample observations (open circles) demonstrates undamped response (see sec. 4.2 for further explanation).

Consider a simple harmonic wave (fig. 9) observed at three sites located at x = 1, 2, and 3. At time t = 1, the wave peak (an arbitrarily identifiable feature) was observed at x = 1, and subsequently at t = 2 and t = 3 was observed at x = 2 and x = 3, respectively. The wave is unchanging in amplitude and moving in the x-direction at constant speed c. Arbitrarily we choose as reference time t = 2. Because data are equally spaced (for simplicity only), the observations from x = 1 and x = 3 at times t = 1 and t = 3 are displaced to x = 2 at t = 2 by application of the time-to-space conversion. Applying the interpolation formula (Eq. 5 in the previous paper) to point x = 2, we find that

$$g(x_2,t_2) = [\eta_1 \cdot f(x_1,t_1)+\eta_2 \cdot f(x_2,t_2)+\eta_3 \cdot f(x_3,t_3)]/(\eta_1+\eta_2+\eta_3) \quad (37)$$

where $\eta_1 = \exp[-(t_1 - t_2)^2/4\nu]$ with similar relationships existing for η_2 and η_3. Note that space weighting does not appear explicity in (37) since $\exp[-(x_2 - x_2)^2/4k] = 1$ and all data are treated as though at x = 2. Recall from the above discussion that $f(x_1,t_1) = f(x_2,t_2) = f(x_3,t_3)$. Therefore, (37) reduces to

$$g(x_2,t_2) = f(x_2,t_2). \quad (38)$$

The response in this case is not a function of either c or ν, as it was in the time-averaging technique. The fundamental difference in the time-to-space

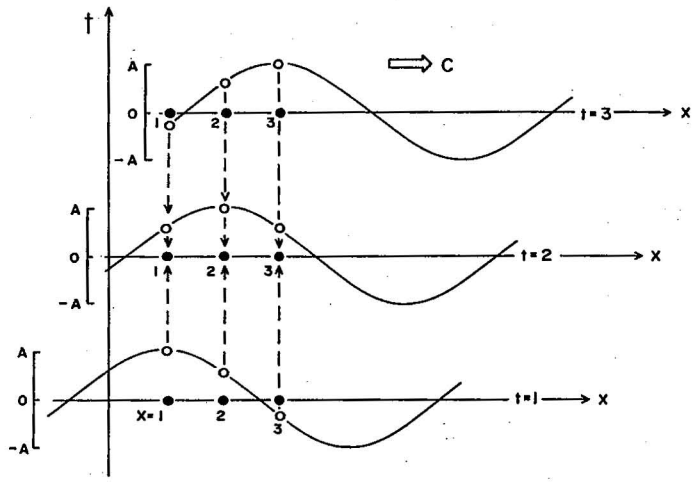

Figure 10. Schematic of time-averaging technique for steadily translating, one-dimensional wave train. Weighting off-reference-time observations t = 1 and t = 3 at same point in space (solid dots) as reference time observation severely damps response to fast-moving, short waves (fig. 6).

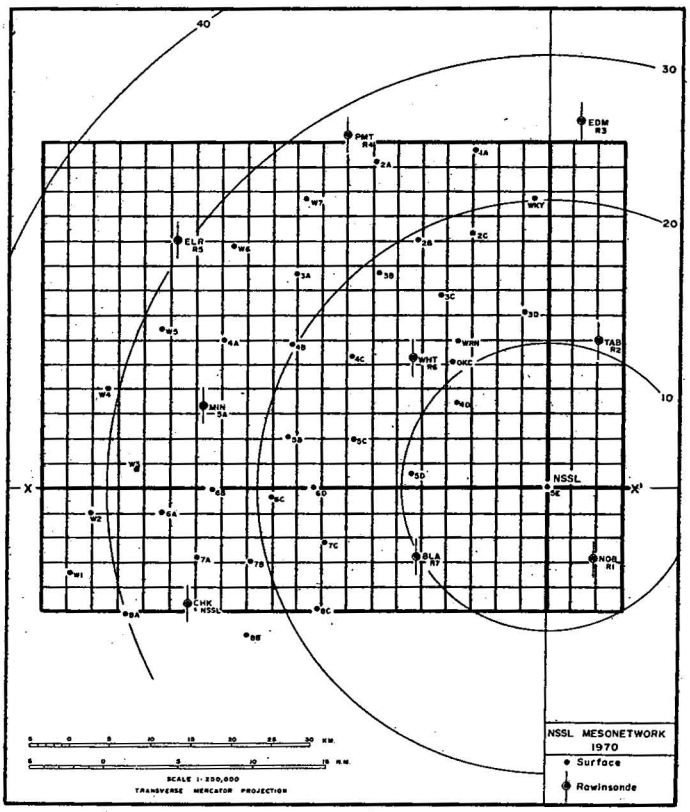

Figure 11. Forty-four station NSSL mesonetwork for 1970. Dots are surface station locations; circles denote rawinsonde sites. Grid shown is 24 by 20 portion of the 36 by 30 surface analysis grid. Mesh size is 3.175 km. Heavy line is X-X' is reference line for figures 12 through 18.

conversion and the time-averaging methods can be seen by comparing figure 10 with figure 9. In figure 10, the same steady-state wave moves past observing sites at x = 1, 2, and 3, but in the time-averaging scheme, the observations at times t = 1 and t = 3 are averaged with the reference-time observations (t = 2). Conservative wave features have not been used to enhance the information content of the observations, but to suppress it. Hence, the strongly damped responses we noted in figures 6 and 7.

5. EMPIRICAL TESTS ON ANALYTICAL DATA

For the empirical tests, a simple analytical function specifies the data observed at an array of sites identical to the 1970 NSSL mesonetwork (fig. 11). The 44 surface stations are spaced at roughly 10 km intervals. To accommodate the displacement of off-time observations along the storm vector, we constructed a 36 by 30 grid with mesh size 3.175 km (equivalent to 0.5 inches on a 1:250,000 map; also a convenient dimension for gridded information on a standard 10 character per inch line printer). For display, only a 24 by 20 portion of the larger grid was used. Dots indicate locations of surface stations and circles rawinsonde sites.

In general, the computer program flows as follows: input weight function parameters and program constants, input disturbance velocity and reference time, input data, perform bookkeeping calculations that locate data in space and time relative to station location and reference time, interpolate data to grid points with a one pass correction (as in sec. 3), output results.

In these tests based on analytical data, the function

$$f(x,y,t) = A \sin[a(x-ct')] \tag{39}$$

determines both the "observed" data and the verification values at grid points. Two wavelengths are studied, both relatively short compared to the station spacing: λ = 20 and 40 km. Wave amplitude A is set equal to 1000 arbitrary units and results are printed to the nearest unit. Both waves move from west (left) at 20 kt.

Observations from all 44 stations are analyzed, but in figures 12 through 18 we show only results along the west-east line X-X' in figure 11. Solid lines are the test curves (39). Dashed lines connect interpolated grid point values using $4k$ = 64 km^2 and 4ν = 900 min^2 with γ = 0.25. Dotted lines are for $4k$ = 36 km^2, 4ν = 70 min^2, and γ = 0.25. The circles at the bottom depict spacing of observation sites within one grid length north or south of line X-X'. The tic marks along the line through the rightmost circle (NSSL) denote relative positions of off-reference-time observations at 5-min intervals. By imagining other lines extending west-east through each station, the increased density of information becomes clear.

According to figure 2, the expected initial responses at 20 km with $4k$ = 64 and 36 km^2 are 0.21 and 0.42, respectively. From figure 3 with γ = 0.25, the corresponding corrected responses are 0.74 and 0.89. In the more densely observed left half of figure 12, the experimental responses are close to the theoretical responses for space weighting. In the more sparsely

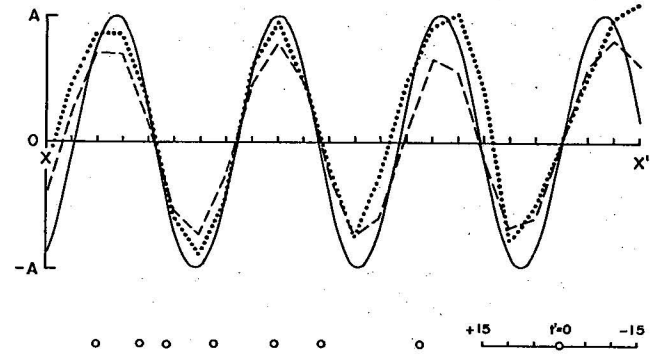

Figure 12. Test response to (39) along line X-X' in figure 11 for 20 km wave moving 20 kt from left to right. Solid line is test function; dashed line connects grid point values using $4k = 64$ km^2, $4\nu = 900$ min^2; dotted line is for $4k = 36$ km^2, $4\nu = 70$ min^2. Both responses were calculated with $\gamma = 0.25$ Circles denote station locations within one grid distance from line X-X'. Tic marks either side of rightmost station circle show relative positions of 5-min interval observations for $\pm$ 15 min from reference time. Identical distribution exist at each of the other stations.

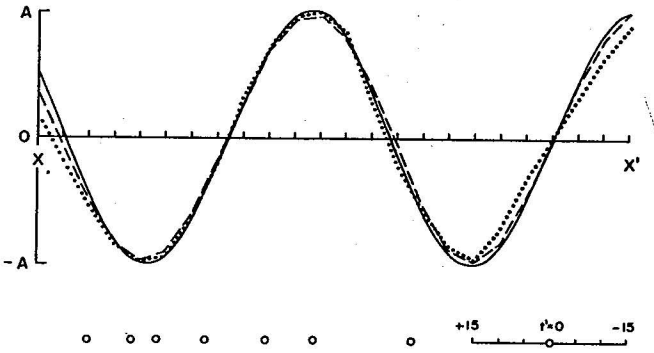

Figure 13. Same as figure 12 except wavelength is 40 km.

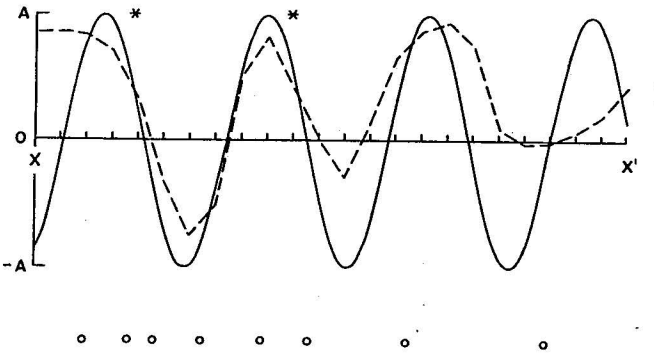

Figure 14. Response to "synoptic" data generated by (39) for 20-km wave. Only data at reference time were considered at each of the 44 stations (fig. 11). Parameters for the analysis are $4k = 64$ km^2 and $\gamma = 0.25$.

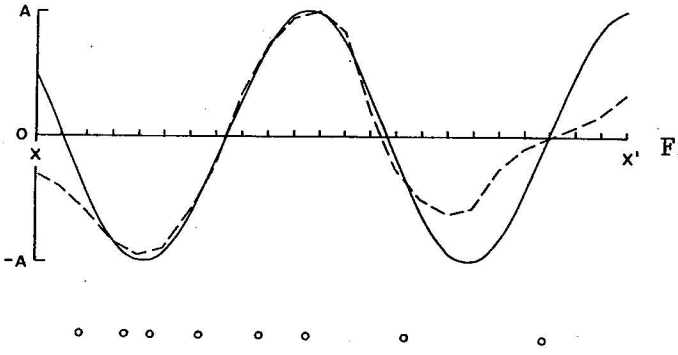

Figure 15. Same as figure 14 except wavelength is 40 km. Compare figure 13.

observed right half, both test result amplitudes and phases are noticeably poorer. The 40 km results (fig. 13) are considerably better than the 20 km results (fig. 12). Both expected and test responses are over 0.95 for the longer wave.

Figures 14 and 15 show results of a more conventional analysis of (39) in which only data observed at the reference time are considered. Parameters used in the analyses are $4k = 64$ km^2 and $\gamma = 0.25$. Except for the region between asterisks in figure 14, the response to the 20 km wave is very poor. The 40 km wave (fig. 15) is well represented except near the left boundary and in the sparsely observed region on the right. Comparing this with figure 13 clearly demonstrates the value of the asynoptic data.

Two other tests using analytical data (39) are relevant in applications to meteorological data. For the 20 km wave, observation frequency was increased to one per minute over a 15-min period at each station to test the sensitivity of the result to the time scale of observations. Weight function parameters and wave speed were the same as those used to produce the dashed curve in figure 12. The result, shown in figure 16, indicates no particular improvement in the representation of the 20 km wave. In retrospect, this result could have been anticipated on the basis of the response curve $4k = 64$ km^2 in figure 2 which indicates nearly zero response for wavelengths smaller than 10 km. Had there been information in the 1-min observations concerning small scale waves, it would have been suppressed, since the total length of the data line (illustrated for the rightmost station in fig. 16) is only 9.3 km.

This exemplifies some points to be considered when choosing the time interval between observations (assuming such a choice is available as with continuously measured surface data). Typically, small scale atmospheric phenomena are also short lived. They may change markedly during passage from one station to the next, or they may pass unobserved between stations, and will not appear in the analyzed result no matter how small the data time interval. In general, details much smaller than the average station separation cannot be depicted by simply clustering time-series observations around stations if large data gaps are left between stations. The weight function should be so designed that it resolves only features well correlated with observations at surrounding stations. Details are most easily improved by increasing the data density uniformly over the analysis area (and at the same time decreasing the mesh size to no more than half the shortest wavelength expected to be resolved.

The final analytical test concerns the effect of errors in determining phase speed. The computer program was modified to create a 25 percent speed error for the 20- and 40 km waves. Consequently, the correct observations (from Eq. 39) were placed at the wrong points in space. There is negligible difference between the "correct" analyses (figs. 12 and 13) and the "erroneous" analyses (figs. 17 and 18), because the speed error produces a 1 km (approx.) relative displacement error between observations. This introduces noise at very small wavelength compared with the wavelength of the test functions, and the response to such small scale noise is essentially zero. Thus, even modest errors (uncertainties) in phase speed have little effect on the analysis of relatively long wave features. The next section considers the effects of errors in both speed and direction as applied to meteorological data.

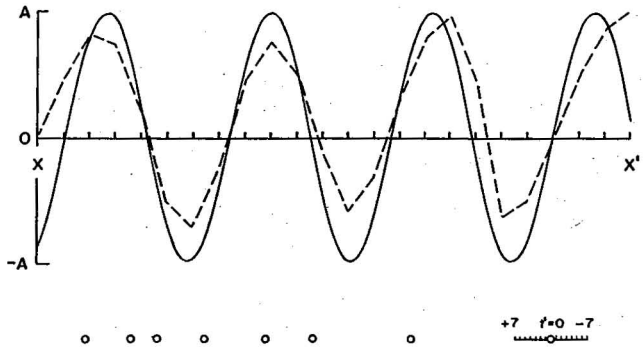

Figure 16. Response to 20-km wave (39) using 1-min data observed over a 15-min period at each station. Compare with dashed curve in figure 12.

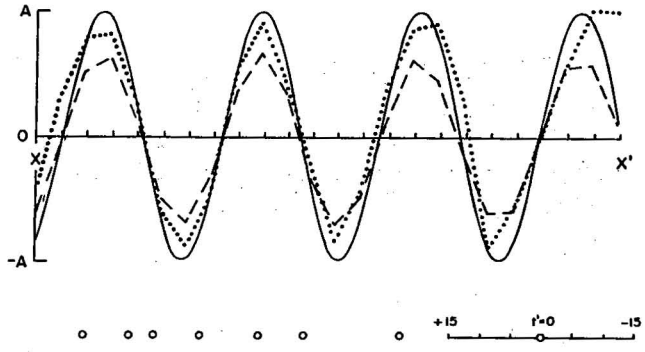

Figure 17. Response test to 20-km wave similar to that in figure 12 except for an artificially induced positioning error in observations due to a 25 percent error in the phase speed.

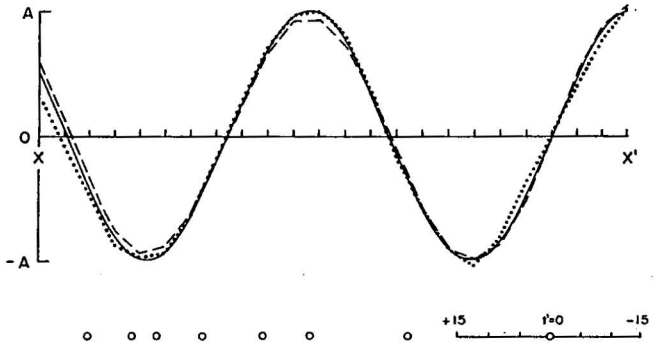

Figure 18. Same as figure 17 except wavelength is 40 km. Compare figure 13.

6. EMPIRICAL TESTS ON METEOROLOGICAL DATA

6.1 Surface Analyses

The analysis scheme was first tested on wind data from the NSSL surface mesonetwork stations for 30 April 1970. An isolated, well-organized thunderstrom producing hail and a tornado passed over the network (fig. 11). This storm's meteorological aspects were discussed in another paper (Barnes, 1972). Here, attention focuses on the analysis scheme's treatment of the data.

Average wind speeds and directions over 5-min intervals were determined manually from autographic records. These data were punched on cards, edited, and then processed by computer to yield gridded and contoured distributions.

The surface wind analysis program is in appendix B. For these studies, phase velocities were determined by the average velocity of the storm's radar echo centroid at 0° antenna tilt. Although an 8-hr ensemble of 5-min observations was available, the surface analysis scheme considers only observations taken within 15 min of the reference map time. Thus, each reporting station generates a sub-set of seven observations per map. When all observations are available, each analyzed field is based on 308 discrete data points. Figure 19 shows the distribution of wind vectors for 0030 CST, 30 April 1970. This particular time was chosen to test the scheme because

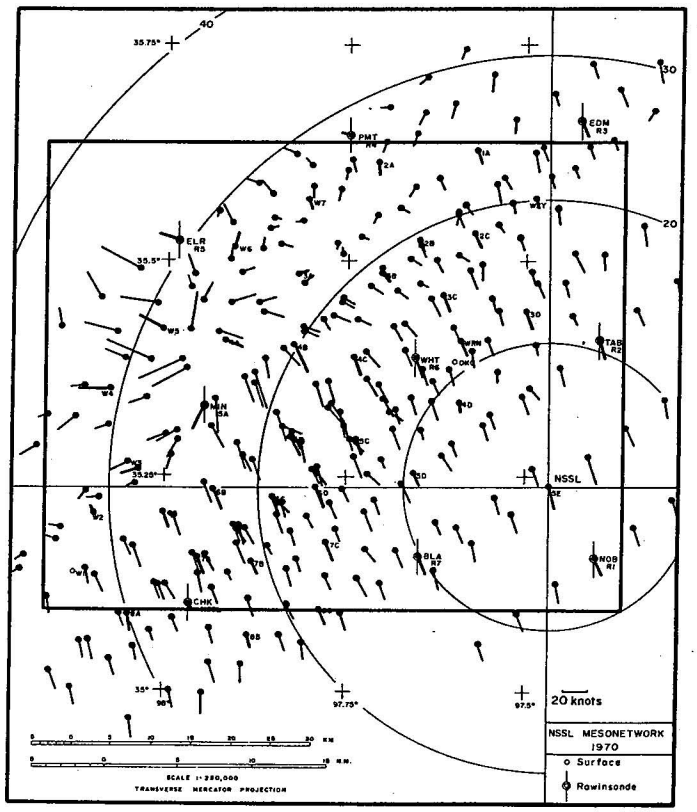

Figure 19. Distribution of surface winds averaged over 5-min intervals for ± 15 min of map time 0030 CST, 30 April 1970. On-time observations are bold vectors projecting in direction from which wind is blowing. Individual spacings of observations along storm vector (233° 41.6 kt) is easily seen at station R1 (NOB) in the southeast corner of grid. Rectangular area encloses 24 x 20 display grid (fig. 11).

flow pattern contains two singular points (a mesocyclone and col) and a shear line (the gust front or pseudo-cold front from the thunderstorm). The 0030 CST observations are drawn as bold vectors (at each station) in the direction from which the wind is blowing. The storm vector for this analysis is from 233° at 41.6 kt. The relative positions of the off-time observations are illustrated clearly by the NOB data in the southeast corner (the 0015 CST data falls just outside the figure northeast of the station).

Wind analysis proceeds in the following manner. Observations are reduced to u and v (magnitudes of easterly and northerly components). These scalars are independently interpolated to the grid points using an equation analogous to (37) with η's corresponding to the exponential part of (19). Then the fields of speed and direction are reconstructed from the analyzed u and v fields. (Storm vector components can be subtracted to yield the flow relative to the storm, but only flow relative to the earth is shown.) For easier visualization, analyzed speeds and directions at grid points are machine plotted as wind vectors; streamlines are sketched manually and the machine-contoured isotachs superimposed.

Analyses of surface wind observations (fig. 19) were tested three ways:

1. using seven observations from each station and $4k = 64\ km^2$, $4\nu = 128\ min^2$, $\gamma = 0.5$;

2. using only reference time observations and $4k = 64\ km^2$, $\gamma = 0.5$;

3. using seven observations from each station but weighing them equally with respect to time by choosing $4k = 64\ km^2$, $4\nu = 99999\ min^2$ (approximates infinity), and $\gamma = 0.5$.

Figures 20, 21, and 22 respectively illustrate these tests and show that the principal differences are the positionings of the circulation center, the col, and the flow near the gust front. The "synoptic" analysis (fig. 21) places the circulation center about 1 km farther west of station 4A than either of the other two tests. The original data records suggest this center passed very close to 4A. Also in figure 21, the col has been extrapolated to a position near the grid boundary, but the analog records suggest that it passed southeast of R5 (winds veered), very near W6 (winds backed) just to the northwest of W7 (winds backed) where the other analyses (figs. 20 and 22) place it. Finally, the treatment of the gust front in the southwest corner of the map is poorer in the "synoptic" analysis where it's indicated near W1 (for which, incidentally, wind data were missing) when actually it had just passed W2 at map time. Also in figure 20 and 22, the flow behind the front in the area west of W2 seems more consistent with that analyzed at later times (not shown) farther into the network area.

It is now quite evident from these tests that time-to-space objective analysis yields significantly more information concerning quasi-steady meteorological patterns than similar analyses of "synoptic" data alone. In fact, considering the redundancy of information displayed in figure 19, it's questionable whether all data were required (or would be required in future networks) to ascertain the significant flow features near large

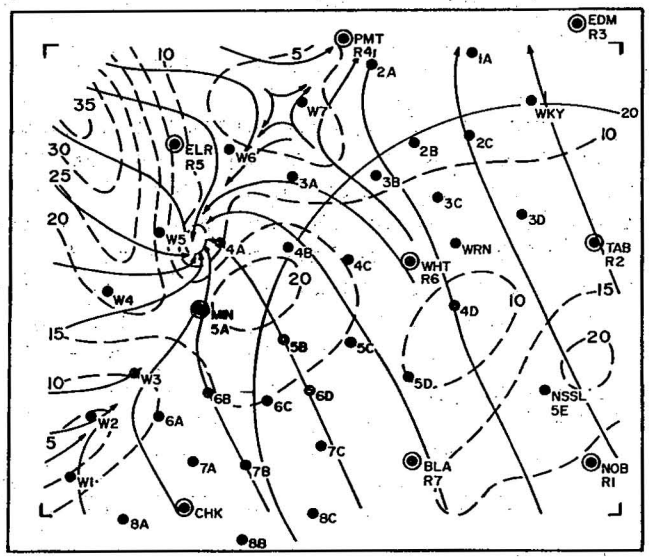

Figure 20. Surface wind analysis at 0030 CST, 30 April 1970, based on observations shown in figure 19 with $4k = 64\ km^2$, $4\nu = 128\ min^2$, and $\gamma = 0.5$.

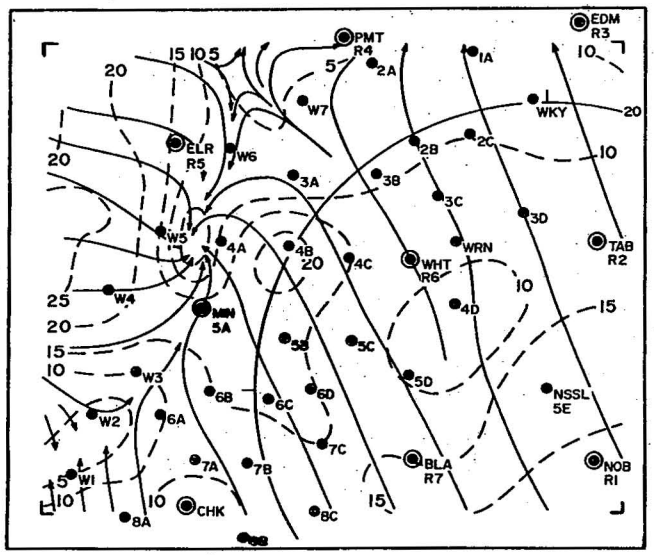

Figure 21. Same as figure 20 except only reference time observations (0030 CST) were used.

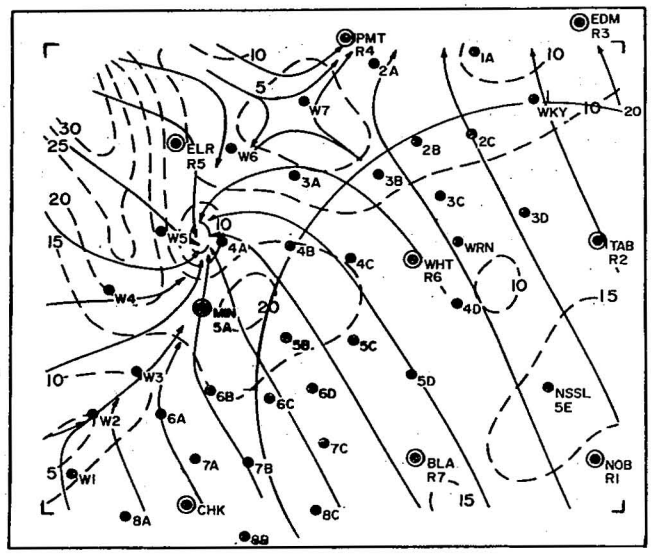

Figure 22. Same as figure 20 except all observations were given equal time weighting as though from a truly steady, translating disturbance.

thunderstorms. This question will be addressed in a later paper.

6.2 Upper Air Analyses

The problems encountered in analyzing sounding data are considerably more complicated than those just described. At the surface, observation sites are fixed and time intervals between data abstracted from continuous recordings can be chosen with considerable freedom. On the other hand, typical NSSL soundings are released at irregular intervals, rise at uncontrollable rates, and drift in various directions (Barnes, Henderson and Ketchum, 1971). Accurate account is kept of the balloon trajectory, but rarely are sufficient data obtained at the same altitude and time to warrant analysis of a given parameter. These problems, inherent in any ensemble of soundings, usually are considered less important to analyses of macroscale data. On the individual thunderstorm scale, it is imperative to consider observations relative to the storm. All of these problems emphasize the need for appropriate objective map analysis techniques.

The relative sparseness of upper air data prevents testing the analysis scheme in the same manner as surface data were tested. Generally there is no information redundancy, and each observation must either be accepted literally or rejected on the basis of observational irregularities, known or unknown. Acceptability of test analyses was determined subjectively from guidance information objectively calculated; i.e., root-mean-square (RMS) differences between interpolated values and observed data for the grid area in the immediate vicinity of the network, and the number of observations for which the interpolated results had not converged to within arbitrary limits. These not only provide information on overall agreement between the analyzed result and observations, but also serve to flag extreme observations. A low noise level (lack of numerous, small extrema and isopleth wiggles) in such gradient-dependent variables as divergence and vorticity also indicates analysis quality. This information further corroborated the quality judgments based on the above calculations, and, therefore, is not presented here.

The test data were observed on 29 April 1970 a few hours prior to the surface test data. (Upper air data at 0030 CST 30 April 1970 were less abundant.) Chosen map times are 1805 and 2240 CST at the 1500 m (MSL) level. This level was chosen because it's above the planetary boundary layer--where natural variations are poorly sampled by the sounding network--but still low enough to retain some link with surface-measured distributions. A small storm entered the network near CHK at 1805 CST, and soon dissipated. At 2240 CST, a larger storm in its mature stage covered the entire central portion of the network along the southwest-northeast diagonal. Both cases were sampled by 15 soundings.

The grid for upper air analyses is 35 by 19 mesh points 6.35 km apart and is oriented along the storm motion vector. The analyses are displayed over the 25 x 17 interior portion of the grid. The center of the grid is always fixed on WHT (Wheatland, Okla.). Figure 23, showing the grid orientation for the 2240 CST storm, illustrates the scale of the computer results to follow.

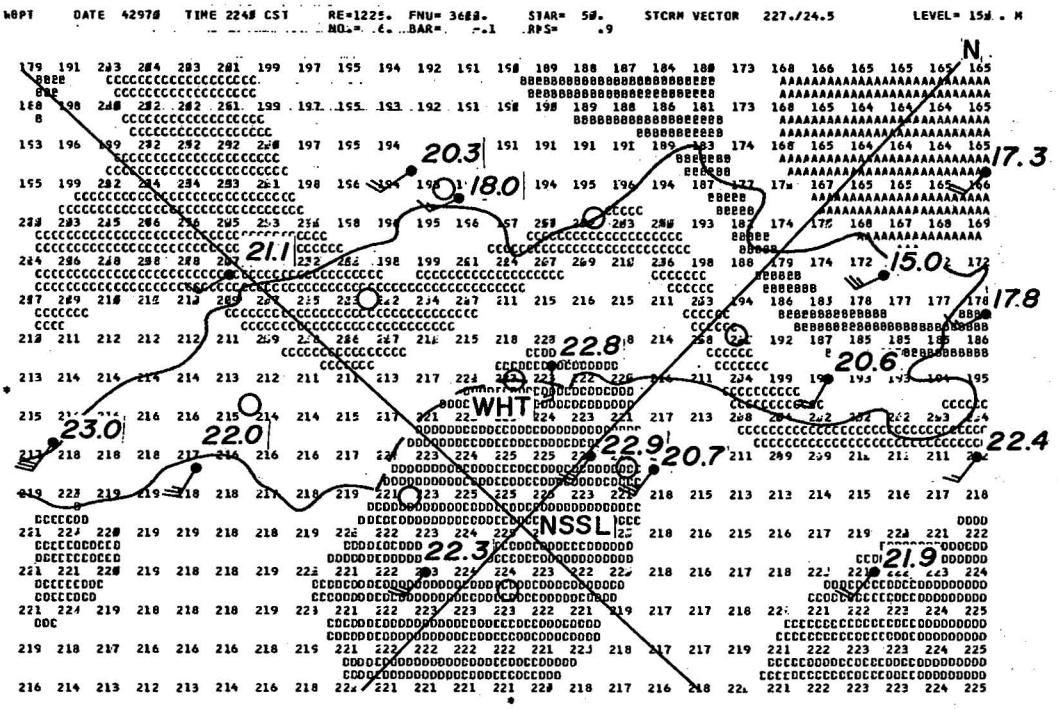

Figure 23. Wet-bulb potential temperature analysis for 2240 CST, 29 April 1970, at 1500 m (MSL) with $4k = 1225\ km^2$, $4\nu = 3600\ min^2$, $V^* = 50\ m\ sec^{-1}$ and $\gamma = 0.343$. Grid values are in tenths °C; isotherms shown by letter shading are every 1°C. Open circles are rawinsonde sites identified in figure 11. Dots show positions of balloons after time-to-space conversion relative to map time. Grid orientation is along 227°-47° line with true north indicated by line N through NSSL. Outline of 1500-m CAPPI radar echo was derived from digital reflectivity data. (Dashed line indicates limit of digital radar data due to ground clutter.) Wind barbs follow convention of one full barb equal to 10 $m\ sec^{-1}$.

In addition to time and space weighting, the upper air data were modified by two other factors. Anisotropic weighting along the wind direction was applied in a manner similar to that suggested by Inman (1970). That is, factor 4k in (19) was modified according to the relationship

$$4k^* = 4k(1 + \beta \cos^2 \phi) \tag{40}$$

where $\beta = V/V^*$, and ϕ is the angle between the position vector, from grid point to observation, and the wind vector V. V^* is some characteristic value of wind speed which, as Saşaki (1971) has shown, should modify the effective radius used in the space weighting by a factor ranging from 1 to about 3. The second modification--first suggested by Sasaki (1958)--includes an additional weight factor reflecting the observation accuracy (representa-

tiveness). Thus, the weight function for the upper air analyses is

$$\eta = \alpha \cdot \exp[-r^2/4k^* - t'^2/4\nu] \tag{41}$$

where $0 \leq \alpha \leq 1$. The α's in this application were assigned arbitrarily upon guidance from quality control information (see Barnes et al., 1971) for individual soundings or upon reviewing results of preliminary analyses (particular attention was given the observations that produced extrema in the divergence patterns). In practice, the quality of thermodynamic data and wind data are evaluated independently. In the 1500-m analyses presented, only two wind observations were discarded ($\alpha = 0$), and two other thermodynamic observations were downgraded slightly ($\alpha = 0.8$ and 0.9) because balloon position data were not available.[2]

Five basic parameters are analyzed from the upper air data (see appendix C for program details): (1) wet-bulb potential temperature calculated by the method of Prosser and Foster (1966), (2) temperature, (3) mixing ratio, (4) u and (5) v wind components (u is defined positive in the direction of storm motion with v positive to the left). Parameters 4k, 4ν, and V* varied over a range of values and the fit (representativeness) of the analyzed fields evaluated by the described methods.

The results are summarized in tables 1 through 3. Analysis variations due to parameter 4k are shown in table 1 for 4k = 196, 441, 784, and 1225 km^2. (These numbers are the squares of 1.4 times 10, 15, 20, and 25 km.)[3] Other parameters were fixed: $4\nu = 3600$ min^2, V* = 50 m sec^{-1}, and $\gamma = 0.343$, a constant for all tests. For each of the five meteorological variables, the upper row of numbers is the RMS difference between the interpolated result and those observations lying within a 14 by 16 grid portion centered at WHT, i.e., in the network area. On the row below is the number of observations that differ from the interpolated result by an amount exceeding the tolerance in parentheses. The total number of observations of each variable appears below that variable's coded name.

As expected, a poorer fit results when 4k is large, and so a considerable portion of the variance is not explainable by the longer wavelengths. On the other hand, with 4k = 196 km^2 observational uncertainties and meteorological

[2]Of the 58 soundings available during these storm periods, data accuracy was suspect ($\alpha < 1$) in portions of only 5 soundings.

[3]The factor 1.4 was chosen for reasons relating to the ratio of weight factor influence radius to average station spacing as developed in the previous paper (Barnes, 1964), but these reasons have lost their relevance in this treatment.

Table 1. Analysis scheme responses to variations of space weight parameter, 4k. NSSL sounding data for 1500 m, 29 April 1970 were used. Number of observations appears below variable's code name.[4] In each row, upper number is RMS difference between analyzed result and observations, lower number is number of observations different from analyzed results by more than tolerance. Parameters 4ν, V*, and γ were constants 3600 min^2, 50 m sec^{-1}, and 0.343.

	Tolerance	4k =	196	441	784	1225 km^2
1805 CST						
WBPT			0.2	0.4	0.6	0.7
10	(± 1°C)		0	0	1	2
T			0.4	0.7	0.9	1.1
10	(±0.5°C)		2	5	8	8
MXR			0.3	0.5	0.7	0.8
10	(±0.5 g kg^{-1})		2	3	5	7
U			0.8	1.3	1.6	1.8
6	(±1 m sec^{-1})		1	3	3	3
V			0.3	0.6	0.9	1.0
6	(±1 m sec^{-1})		0	2	2	2
2240 CST						
WBPT			0.4	0.6	0.8	0.9
6	(±1°C)		0	0	3	2
T			0.1	0.3	0.4	0.5
6	(±0.5°C)		0	1	1	1
MXR			0.5	0.9	1.1	1.3
6	(±0.5 g kg^{-1})		3	4	4	5
U			0.3	1.3	2.4	3.4
6	(±1 m sec^{-1})		0	2	3	3
V			0.8	1.3	1.6	1.8
6	(±1 m sec^{-1})		2	2	4	4

[4]Wet-bulb potential temperature (WBPT), temperature (T), mixing ratio (MXR), wind components along and to left of storm's translation vector (U and V).

Table 2. Empirical responses for variations of time weight parameter, 4ν. Parameters 4k and V* were held constant at 441 km^2 and 50 m sec^{-1}, respectively. See table 1 for additional explanation.

	Tolerance	4ν = 225	900	3600	8100	$10^6 min^2$ ($\rightarrow\infty$)
		1805 CST				
WBPT		0.8	0.4	0.4	0.4	0.4
10	($\pm$1°C)	3	0	0	0	0
T		1.3	0.7	0.7	0.7	0.7
10	($\pm$0.5°C)	5	4	5	4	5
MXR		0.9	0.5	0.5	0.5	0.5
10	($\pm$0.5 g kg^{-1})	4	3	3	3	3
U		2.4	1.7	1.3	1.3	1.2
6	($\pm$1 m sec^{-1})	2	3	3	3	3
V		1.2	0.7	0.6	0.6	0.6
6	($\pm$1 m sec^{-1})	1	1	2	2	2
		2240 CST				
WBPT		0.9	0.7	0.6	0.6	0.6
6	($\pm$1°C)	2	2	0	0	0
T		0.5	0.3	0.3	0.3	0.3
6	($\pm$0.5°C)	1	1	1	1	1
MXR		1.4	1.0	0.9	0.9	0.9
6	($\pm$0.5 g kg^{-1})	3	3	4	4	4
U		1.5	1.4	1.3	1.3	1.3
6	($\pm$1 m sec^{-1})	2	2	2	2	2
V		1.5	1.3	1.3	1.3	1.3
6	($\pm$1 m sec^{-1})	2	2	2	2	2

Table 3. Empirical responses for variations of anisotropic weight parameter, V*, which increases influence of observation along direction of wind (see Eq. (40)). Parameters 4k and 4ν were held constant at 441 km^2 and 3600 min^2, respectively. See table 1 for additional explanation.

		1805 CST							
		V* ($m\ sec^{-1}$)							
	Tolerance	1	10	20	30	40	50	75	100
WBPT		1.0	0.6	0.5	0.5	0.4	0.4	0.4	0.4
10	(±1°C)	3	1	0	0	0	0	0	0
T		1.3	1.0	0.9	0.8	0.7	0.7	0.6	0.6
10	(±0.5°C)	9	7	7	6	7	5	5	4
MXR		1.2	0.7	0.6	0.6	0.5	0.5	0.5	0.5
10	(±0.5 $g\ kg^{-1}$)	7	5	3	3	3	3	3	3
U		2.4	1.6	1.4	1.4	1.4	1.3	1.3	1.3
6	(±1 $m\ sec^{-1}$)	5	3	3	3	3	3	3	3
V		1.4	0.9	0.7	0.7	0.7	0.6	0.6	0.6
6	(±1 $m\ sec^{-1}$)	3	2	2	2	2	2	1	1
		2240 CST							
WBPT		1.2	0.7	0.7	0.7	0.6	0.6	0.6	0.6
6	(±1°C)	2	1	1	0	0	0	0	0
T		0.6	0.3	0.3	0.3	0.3	0.3	0.3	0.3
6	(±0.5°C)	2	1	1	1	1	1	1	1
MXR		1.7	1.0	0.9	0.9	0.9	0.9	0.9	0.9
6	(±0.5 $g\ kg^{-1}$)	5	4	4	4	4	4	4	4
U		4.6	2.0	1.6	1.4	1.4	1.3	1.2	1.2
6	(±1 $m\ sec^{-1}$)	6	3	2	2	2	2	2	2
V		2.6	1.5	1.4	1.3	1.3	1.3	1.3	1.3
6	(±1 $m\ sec^{-1}$)	4	4	4	3	2	2	2	2

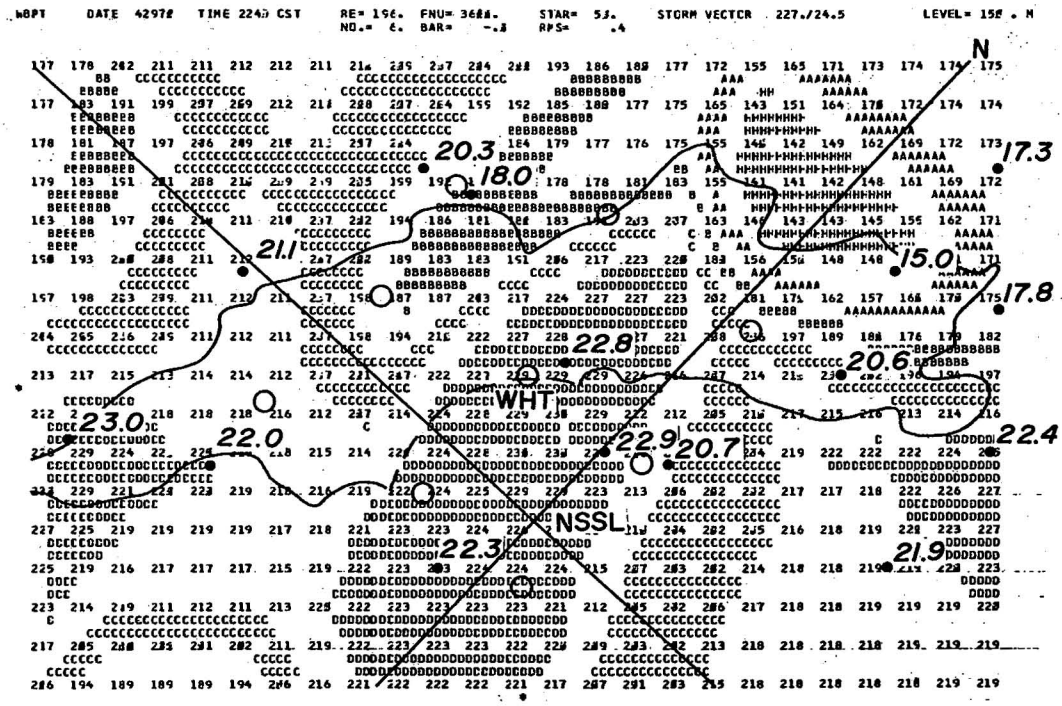

Figure 24. Same as figure 23 except 4k = 196 km^2.

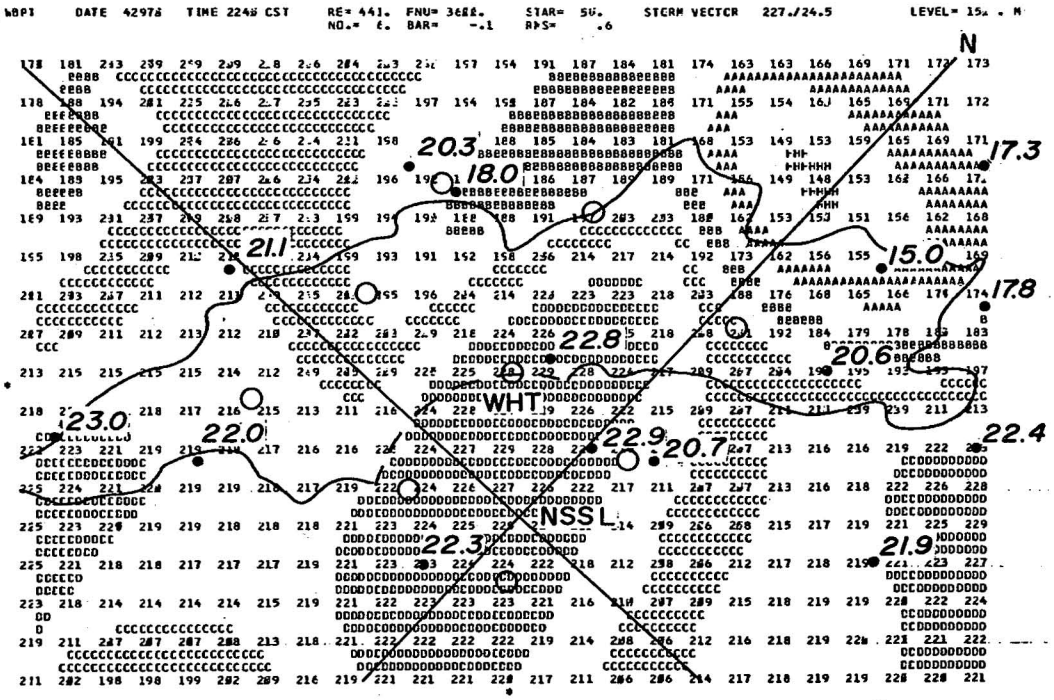

Figure 25. Same as figure 23 except 4k = 441 km^2.

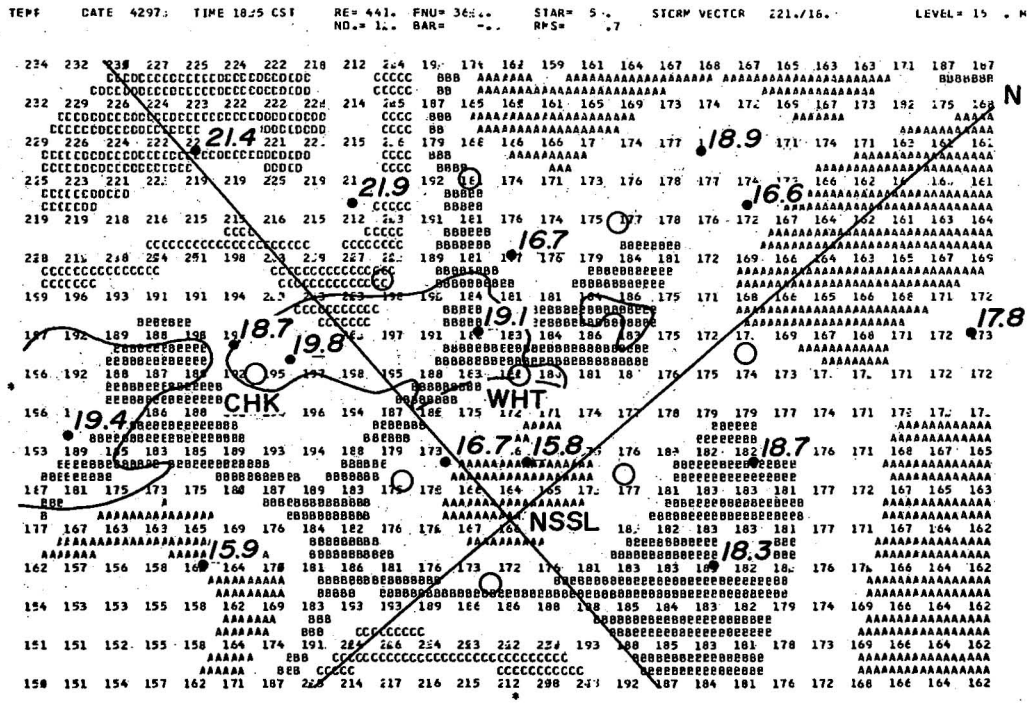

Figure 26. Temperature analysis at 1500 m (MSL) for 1805 CST, 29 April 1970, with $4\nu = 3600$ min^2. See figure 23 for symbol convention.

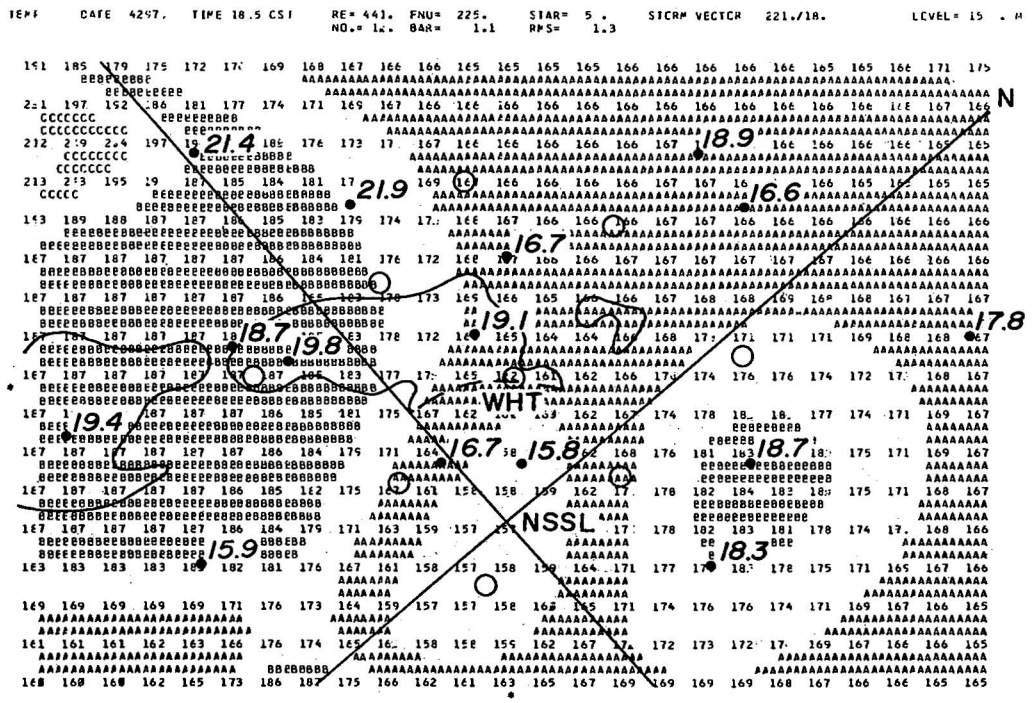

Figure 27. Same as figure 26 except $4\nu = 225$ min^2.

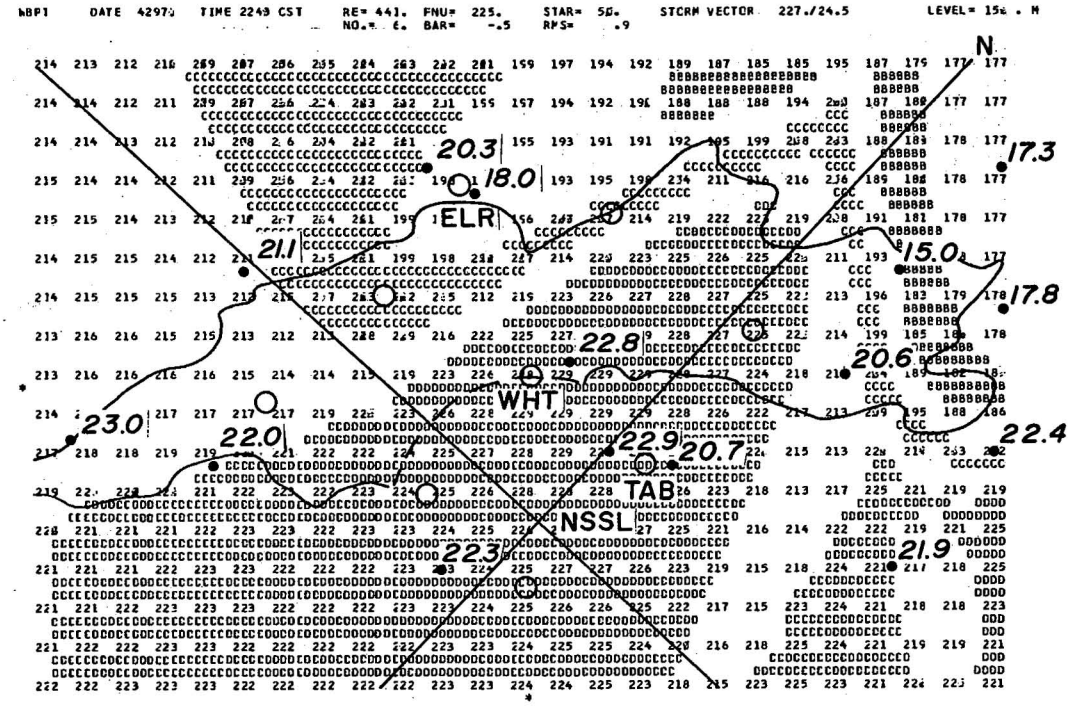

Figure 28. Wet-bulb potential temperature at 2240 CST with $4\nu = 225$ min^2. Compare with figure 25.

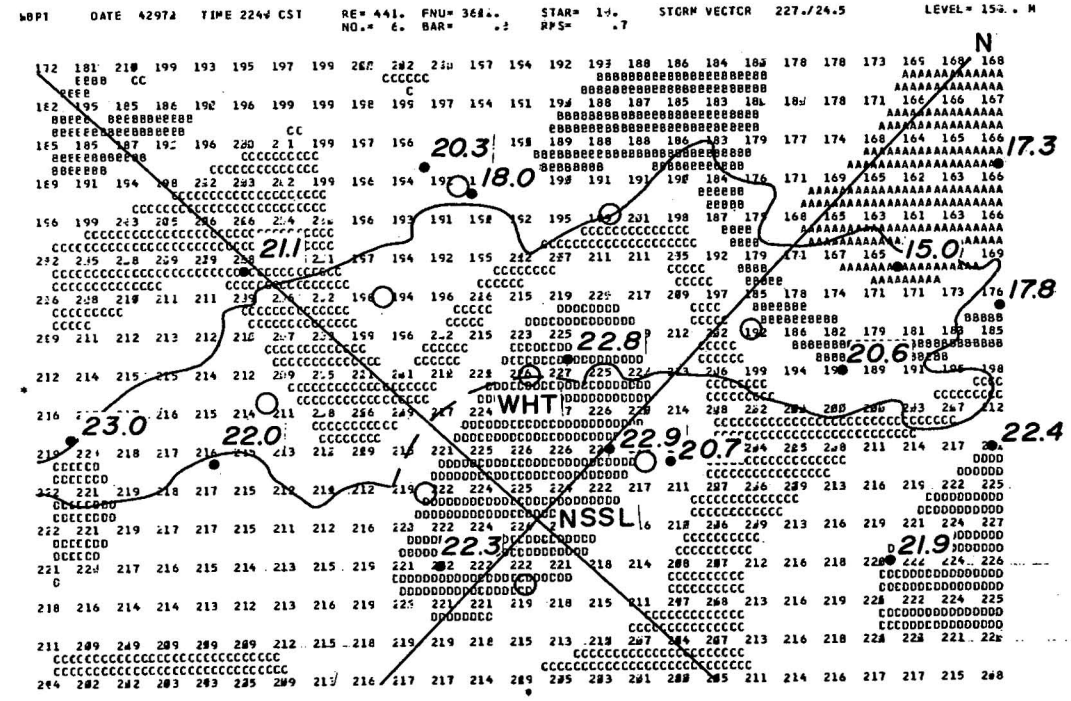

Figure 29. Wet-bulb potential temperature at 2240 CST with $V^* = 10$ m sec^{-1}. Compare with figure 25.

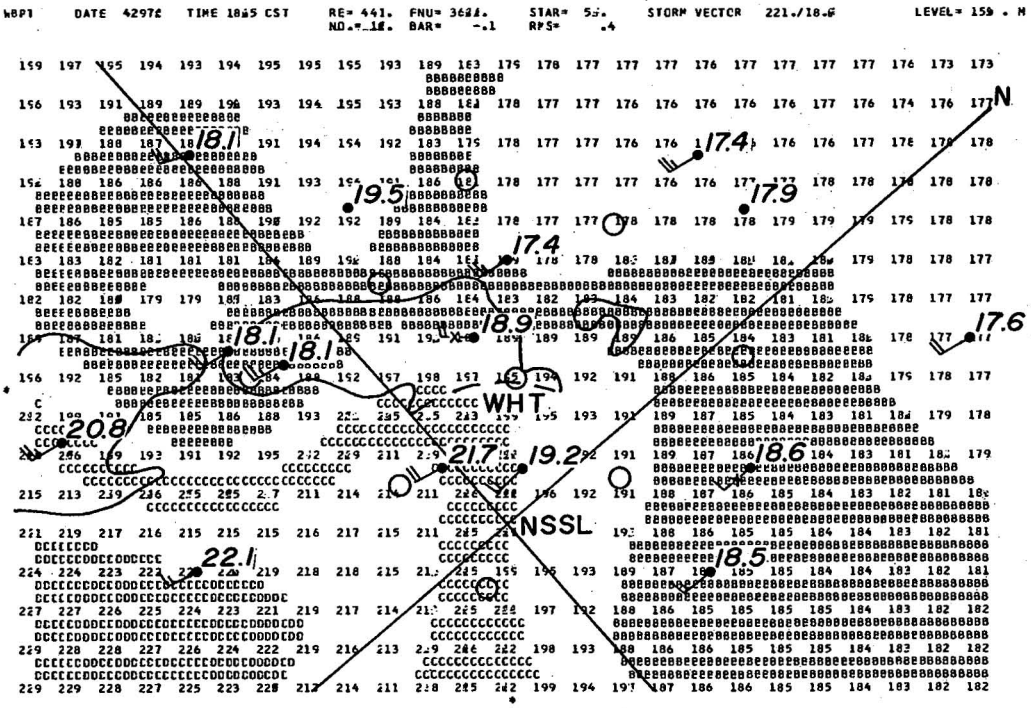

Figure 30. Wet-bulb potential temperature for 1805 CST with actual storm vector determined from echo centroid motion. Compare with figure 31.

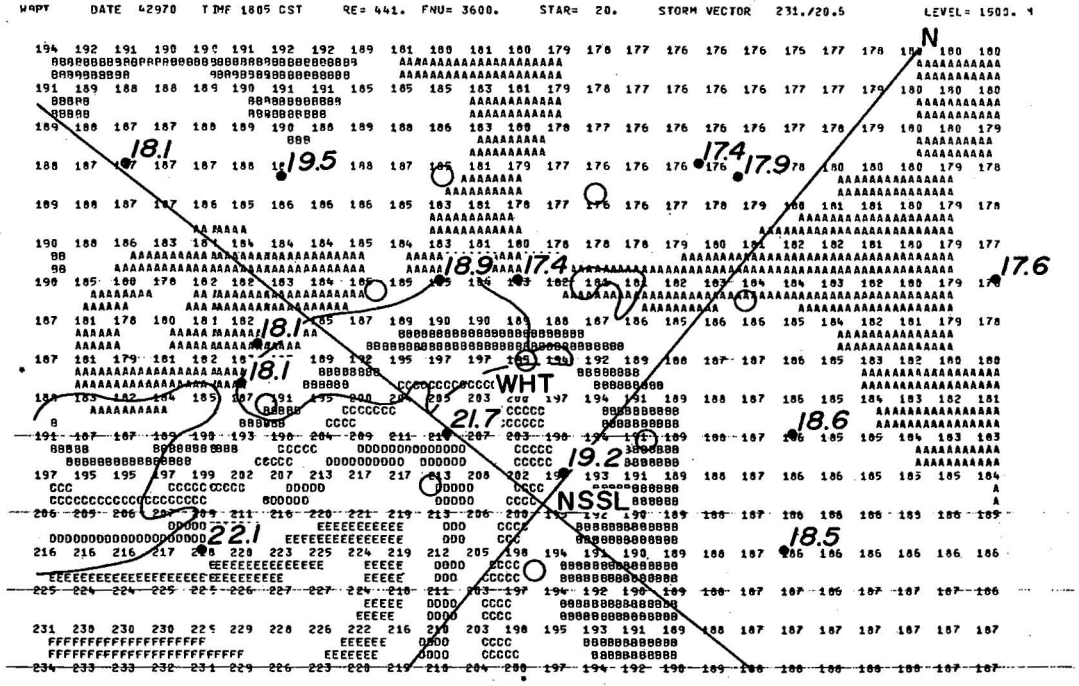

Figure 31. Wet-bulb potential temperature for 1805 CST with "erroneous" storm vector which differs from actual vector by 10° and 2.6 m sec^{-1} (5 kt). Note contour interval is one-half that shown in figure 30. Analysis differences in the network are judged to be minor.

"noise" are retained. These extremes are illustrated in figures 23 and 24 for the 1500-m wet-bulb potential temperature distribution at 2240 CST. Circles are rawinsonde release sites, dots are balloon positions after time-to-space conversion relative to map time, and the 1500 m radar echo is outlined by the solid curve. The cross passes through the radar site at NSSL and denotes the orientation of true north.

Although the analyzed distributions, inside the radar echo are not to be accepted literally (insufficient observations to describe even general details), certain aspects of the storm's WBPT distribution are substantiated when referenced to the more detailed surface observations (see Henderson, 1972). For instance, the observation of high WBPT near WHT is known to be associated with a large vigorous updraft, and the area of minimum WBPT north of the echo (upper right corner of grid) resulted from locally sinking mid-level air. In the analyzed depictions, figure 24 seems to represent the extent of these features better than figure 23. However, considering the possible influence of less certain data, it seems advisable to relax the analysis fit obtained with $4k = 196$ km^2 and use $4k = 441$ km^2 as the "standard" for other tests (fig. 25). Within a reasonably broad range, the chosen value of 4k isn't very critical.

The analysis response to variations in 4ν can be anticipated only in a general sense. Choosing $4\nu = 225$ min^2 is similar to a "synoptic" analysis because observations older than $\pm$ 15 min from map time weigh insignificantly. With 4ν essentially infinity ($= 10^6$ min^2), a steady, translating system is implied, and all observations are weighed without regard to time. It follows if 4ν is chosen somewhere between these values, a quasi-steady system is implied, and the validity of the analysis response can be determined only by trial where no knowledge exists as to the actual steadiness of the disturbance.

Table 2 indicates significant reduction of variance as 4ν is changed from 225 to 900 min^2. There is a little improvement from 900 to 3600 min^2, and almost no change thereafter. The test standard was chosen as $4\nu = 3600$ min^2.

A particularly interesting comparison of time weighting effects is illustrated by 1805 CST temperature analyses in figures 26 and 27. A small thunderstorm just entered the network, produced pea-sized hail at CHK, and dissipated immediately afterward. At 1805 CST, surface wind data indicated a moderate downdraft under the radar echo and no organized updraft. The surface wet-bulb potential temperature pattern (not shown) appeared confused (many extrema). Considering the decaying stage of this storm, one might expect similarly confused thermal patterns extending aloft. Figure 26 is not disappointing. (The pattern's meteorological significance, if at all discernible, will be reported in a future paper.) Here's the point--when little weight is given to off-time observations, the pattern is remarkably flat, and the agreement between analysis and observations is relatively poor (fig. 27). When the off-time data are influential, the analysis agrees more closely with all observations. The key to "goodness" of fit in this case is indicated by the average differences ("BAR") between interpolated values and observed data. For figure 26, BAR is nominally zero, but in figure 27 it is 1.1°C. Moreover the RMS differences are significantly higher in figure 27 although

the number of observations failing the limit test (table 2) is still five (but not the same five).

The 2240 CST WBPT analysis (fig. 28) with $4\nu = 225$ min^2 exhibits a similar lack of detail compared to the analysis standard, figure 25. Also, average and RMS differences are higher in the network area.

In figure 28, there are two notable examples of analysis response to closely-spaced observations at different times. The values 20.3°C and 18.0°C near ELR were observed 4 and 17 min from map time. Near TAB the values 22.9°C and 20.7°C were observed 5 and 26 min from map time. With $4\nu = 225$ min^2, the analyzed values around those two stations are largely dominated by the observations nearer map time. On the other hand, more distance (in time) observations exert considerably greater influence when $4\nu = 3600$ min^2 (fig. 25). Consequently, as reference time changed, the figure 25 pattern was more nearly conserved.

The effect of along-the-wind enhancement (ellipticity) of the weight function was investigated by varying V* between 1 and 100 m sec^{-1}. Table 3 indicates that the analysis fit for V* = 1 m sec^{-1}, relatively poor, improves markedly from V* = 10 to 20 m sec^{-1}, and remains rather uniform during further increases in V*. Generally patterns obtained with V* = 1 m sec^{-1} lacked detail. With V* = 10 m sec^{-1} details improved somewhat but weren't satisfactory. The example in figure 29 shows the WBPT field at 2240 CST. Compare this with figure 25. A significant difference is noted in the minimum center north of the echo. These results suggest caution when applying anisotropic weight functions based on wind direction alone. They don't always improve thermodynamic analysis.

Finally, several tests determined analysis sensitivity to uncertainties in the storm translation vector governing off-time observation displacement. Figures 30 and 31 illustrate the relatively small pattern changes in 1805 CST WBPT effected by an "error" in the storm vector of 10° and 2.6 m sec^{-1} (5 kt). Comparing the values analyzed at stations, the average difference is about 0.3°C. The pattern differences are considered likewise insignificant. (Note that the figure 31 grid is rotated clockwise relative to true north, and the contour interval is 0.5°C, whereas it is 1.0°C in figure 30. Figure 31, an early display program result, has V* = 20 m sec^{-1}. However, we've seen that results with V* = 50 m sec^{-1} aren't significantly different.)

7. CONCLUDING REMARKS

Several methods proposed recently assimilate asynoptic data into analysis and prediction schemes (Miyakoda and Talagrand, 1971; Talagrand and Miyakoda, 1971; Bengtsson and Gustavsson, 1971). These computationally sophisticated schemes generally position data according to a suitable prediction equation and assign weights to the observations according to their "age." Weights are determined empirically in a manner similar to this study--by finding some suitable minimum in the RMS residuals between analyzed-versus-observed values.

The "prediction" equation for positioning observations in this analysis scheme is a simple one-dimensional advection equation with constant advection velocity. So far, applications have been restricted to distributions associated with phenomena that are long-lived relative to the interval between observations. The principal advantages of this scheme are that the response to various scales can be selected to accommodate (or take advantage of) pre-existing information regarding the phenomenon's physical attributes or the peculiarities of the data set, and computational simplicity makes it a useful tool for analyzing a wide range of geophysical phenomena whose complicated physical interrelationships are poorly understood.

The mesoscale upper air analyses presented here are considered to be only a "first look." To date, each physical parameter has been analyzed independently and without constraints on its vertical distribution. Hopefully, this simple technique will provide useful information suggesting methods for amalgamating the different variables into dynamically consistent analyses. The more sophisticated treatments likely will be based on variational schemes now being developed by several investigators (e.g., Sasaki, 1970).

8. ACKNOWLEDGEMENTS

Professor Yoshikazu Sasaki, my teacher and friend for 16 years, is responsible for some of the mathematical derivations in sections 2 and 4.1. My own understanding of the analytical examples was greatly enhanced by our many conversations.

Dr. Gary Achtemeier's comments and suggestions were most constructive, particularly in developing the discussion relating to $\hat{r}' = \hat{c}t'$ in section 4.2. Dr. Edwin Kessler, Director, NSSL, and Joe Schaefer helpfully reviewed the draft.

Helen Ardrey and Joan Myers have made the reader's burden more bearable by their many suggestions regarding style. Typescript preparation fell to Brenda Courtney--her outstanding skill and attention to detail made the production process noticeably smooth. Jennifer Farris, Charles Clark and David Jones did an excellent job producing the graphics, in some cases from originals of poor quality.

To my colleagues who patiently awaited completion of this work, my thanks for your encouragement and questions.

9. REFERENCES

Abramowitz, M., and I. A. Stegun, eds., 1965: Handbook of Mathematical Functions, (Dover Publications, Inc., New York, New York).

Barnes, S. L., 1964: A technique for maximizing details in numerical weather map analysis, J. Appl. Meteor., 3, No. 4, 396-409.

Barnes, S. L., J. H. Henderson, and R. J. Ketchum, 1971: Rawinsonde observation and processing techniques at the National Severe Storms Laboratory, NOAA Tech. Memo. ERL NSSL-53, Norman, Oklahoma, 246 pp.

Barnes, S. L., 1972: Morphology of two tornadic storms: an analysis of NSSL data on April 30, 1970, Preprints of Papers, 15th Radar Meteorology Conference, Champaign, Ill., Amer. Meteor. Soc., 69-76.

Bengtsson, L., and N. Gustavsson, 1971: An experiment in the assimilation of data in dynamical analysis, Tellus, 23, 328-336.

Cressman, G. P., 1959: An operational objective analysis system, Mon. Wea. Rev., 87, 367-374.

Fujita, T., 1963: Analytical mesometeorology: a review, Meteor. Monographs, 5, No. 27, 77-125.

Henderson, J. H., 1972: A detailed description of the internal structure of a thunderstorm, Preprints of Papers, 15th Radar Meteorology Conf., Champaign, Ill., Amer. Meteor. Soc., 61-68.

Inman, R. L., 1970: Papers on operational objective analysis schemes at the National Severe Storms Forecast Center, NOAA Tech. Memo. ERL NSSL-51, Norman, Oklahoma, 91 pp.

Miyakoda, K., and O. Talagrand, 1971: The assimilation of past data in dynamical analysis, I, Tellus, 23, 310-317.

Muller, F. B., 1966: Mesometeorology and short-range forecasting - Report No. 1, Notes on the meteorological application of power spectrum analysis, Canadian Meteor. Memoirs No. 24, Dept. of Transport, Toronto, 84 pp.

Panofsky, H. A., and G. W. Brier, 1958: Some Applications of Statistics to Meteorology (Pennsylvania State University, University Park, Penn).

Prosser, N. E., and D. S. Foster, 1966: Upper air sounding analysis by use of an electronic computer, J. Appl. Meteor., 5, 296-300.

Sasaki, Y., 1958: An objective analysis based on the variational method, Jour. Met. Soc. Japan, 36, No. 3, 77-88.

Sasaki, Y., 1960: An objective analysis for determining initial conditions for the primitive equations, Tech. Rep. (Ref. 60-16T), Dept. Oceanography and Meteorology, Texas A&M University, 22 pp.

Sasaki, Y., 1970: Numerical variational analysis with weak constraint and application to surface analysis of severe storm gust, Mon. Wea. Rev., 98, No. 12, 899-910.

Sasaki, Y., 1971: A theoretical interpretation of anisotropically weighted smoothing on the basis of numerical variational analysis, Mon. Wea. Rev., 99, No. 9, 698-708.

Shuman, F. G., 1957: Numerical methods in weather prediction: II. Smoothing and filtering, Mon. Wea. Rev., 85, 357-361.

Talagrand, O., and K. Miyakoda, 1971: The assimilation of past data in dynamical analysis, II, Tellus, 23, 318-327.

APPENDIX A

Comparison of Analysis Techniques

Analyses of upper air observations (figs. 23 and 30) tested Cressman's (1959) weight function against the weight function defined by (41) to determine their relative merits. Computer programs were identical except subroutine INTERP (see appendix C) was replaced by one incorporating the Cressman weight function

$$W = (R^2 - d^2)/(R^2 + d^2). \qquad \text{(A1)}$$

R is the influence radius and d is the distance from grid point to observation. A short computation developing statistics for grid point values was added to both subroutines (not shown in appendix C).

The manner in which (41) was applied makes it equivalent to (2), the space weight function. All data were treated as though observed simultaneously; time weighting was suppressed by setting $4\nu = 10000$ min^2. Along-the-wind enhancement was also suppressed by V* = 1000 kt. Space weight factor $4k = (21 \text{ km})^2$ and $\gamma = 0.343$.

To make the initial Cressman weight nearly equivalent to the above weight, we set $W = e^{-1}$, let d be some proportion of R such that $d = pR$ where $0 < p < 1$, and solved (A.1) for p. The result p = 0.68 required R = 30.86 km or, since the mesh size is 6.35 km, R = 4.86 grid lengths. This value is comparable to the 4.75 grid lengths Cressman used for initial R in large-scale operational analyses. On each of two succeeding scans, R was decreased by one grid length. We adopted Inman's (1970) requirement that no fewer than two observations should determine a grid point value, thus R may locally increase to be greater than the assigned influence radius for the current scan. Grid point values were not smoothed in either technique.

Five variables were analyzed for each of two data sets: 1805 CST and 2240 CST at 1500 m altitude. We tested the statistical agreement between analyzed results and observations on the one hand, and the pattern of analyzed gridded values on the other. Table A1 summarizes these tests.

For each analyzed variable, observations within $\pm$ 7 grid points of WHT (fig. 23) are compared to the field value bi-linearly interpolated from the four adjacent grid point values to the data point. The "Data Point" statistics are as described in section 6.2. The "Grid Point" statistics are derived from the 425 analyzed values. Mean (AVG) and variance (VAR) have their usual definitions. The rightmost column is an estimate of the local field curvature. The absolute value of the Laplacian (sans division by the grid length squared) was calculated from the five values adjacent to and including each grid point:

$$\text{LAP} = |g(x+1,y) + g(x-1,y) + g(x,y+1) + g(x,y-1) - 4g(x,y)|. \qquad \text{(A2)}$$

These values, averaged over 425 points, indicate the noisiness, or lack of point-to-point correlation, of the analyzed fields.

Except for the "LAP" column entires, the statistics from the two weightin techniques are in close agreement. The RMS values for Cressman weighting average 20 percent smaller, indicating that method coverges more rapidly to the observations in these tests. However, by obtaining closer fit at data points, Cressman weighting generates considerable noise throughout the rest of the field. In every test but one, the point-to-point curvature is at least two times greater. Also, the Cressman field variance averages 14 percer higher for the 2240 CST data set.

The need for additional smoothing of Cressman-weighted results is understandable. However, this cosmetic destroys the advantage of rapid convergence to observations, since the agreement at data points will be compromised by the smoothing filters. Furthermore, additional smoothing necessitates longer computation times, and in these tests the abbreviated Cressman technique already requires 10 percent longer execution time. The more efficient techniq described in this paper converges directly (one iteration) and smoothly to the desired pattern correlation, and its versatility in accommodating asynopti observations increases its value as an analysis tool.

Table A1. Comparison of analyses using weight function (41) versus Cressman weighting technique based on data plotted in figures 23 through 31. Data point statistics include number of observations in network area, average difference (BAR), and RMS difference between observed data and analyzed value at same point. Grid point statistics include mean (AVG), variance (VAR), and the average absolute Laplacian (LAP) of the 425 grid point values for each map. See table 1 for additional conventions.

		1805 CST					
		DATA POINTS			GRID POINTS		
	Technique	No.	BAR	RMS	AVG	VAR	LAP
WBPT	Cressman	10	0.0	0.2	18.9	1.5	0.48
	Eq. (41)	10	0.0	0.3	19.0	1.5	0.23
T		10	0.0	0.4	18.2	1.7	0.79
		10	0.1	0.5	18.1	1.7	0.36
MXR		10	0.0	0.3	8.5	2.2	0.63
		10	0.0	0.4	8.6	2.2	0.28
U		6	0.3	0.9	18.3	3.7	1.67
		6	0.4	1.1	18.2	3.4	0.60
V		6	0.0	0.4	10.4	2.3	1.06
		6	0.0	0.5	10.3	2.3	0.44
		2240 CST					
WBPT	Cressman	6	0.0	0.5	20.5	2.4	0.92
	Eq. (41)	6	0.0	0.6	20.6	2.1	0.41
T		6	0.0	0.2	17.4	1.7	0.77
		6	0.0	0.3	17.4	1.4	0.34
MXR		6	-0.1	0.7	10.8	3.5	1.34
		6	0.0	0.9	10.9	3.1	0.60
U		6	-0.1	0.8	13.3	4.8	2.53
		6	-0.1	1.1	13.4	3.8	1.29
V		6	-0.1	1.1	14.3	4.9	1.98
		6	-0.1	1.3	14.4	4.5	0.88

APPENDIX B

Surface Wind Analysis Program

This program is written in FORTRAN IV language. The main program inputs data from a previously prepared magnetic tape (device 4), reads from cards (device 5) the output device number (LO), total number of observations per station in the data bank (NTOBS), weight function parameters (4k = RE, 4ν = FNU; see (19)), number of observations per station to be included in each map analysis (NT), storm direction and speed (SD,SS), reference time (NTIME), and date (IDT). After bookkeeping calculations for the time-to-space conversion of data points, the program calls subroutines which accomplish the interpolation to grid points (INTERP), divergence (DIV) and vorticity (VORT) calculations, and outputs contoured maps of the analyzed fields (CONTUR).

```
C    SURFACE ANALYSIS WITH TIME-SPACE CONVERSION
C            FOR SURFACE WIND FIELD, ACTUAL AND RELATIVE
      DIMENSION STA(44),IT(109), DIR(44,109),SPD(44,109),U(44,109),
     1  V(44,109),                          DX(07),DY(07),XS(44),YS(44),
     2 KK(6),DGP(36,30),SAVE(36,30)
      COMMON KT(07),DT(07),XL(44,07),YL(44,07),IMIN(44,07),
     1  JMIN(44,07),MAP(24,20),RE,FNU,SU,SV,UR(24,20),VR(24,20),NT,LO
      DATA KK/4H   U,4H    V,4H SPD,4H DIR,4H DIV,4HVORT/
      DATA XS/-9.83,-2.55,-22.43,-16.81,-8.92,-32.29,-22.12,-14.23,
     1-3.,-41.54,-33.20,-11.80,-25.46,-11.96,-43.97,-33.5,-25.16,-17.42,
     20.,-48.98,-42.76,-35.63,-30.32,-44.58,-38.20,-28.34,-53.38,-45.49,
     3-38.20,-29.71,-60.51,-57.63,-52.77,-56.11,-49.58,-40.03,-31.23,
     45.34,5.95,3.37,-26.07,-47.46,-17.42,-17.12/
      DATA YS/43.49,37.01,41.63,31.82,32.19,27.75,27.75,24.97,22.56,
     118.86,18.86,18.86,17.19,10.89,10.71,6.26,6.07,2.0,0.0,-3.74,-0.41,
     2-0.78,-0.04,-8.56,-9.48,-7.08,-16.52,-15.04,-18.93,-15.97,-11.15,
     3-3.56,2.18,12.56,20.34,30.71,37.01,-8.93,19.04,47.38,45.53,32.01,
     417.19,-8.56/
      DEL=8.1015
      RAD=57.29578
      CT=0.15444
      READ(5,996)LO,NTOBS
996   FORMAT(I2,I3)
20    READ(4,100)((STA(N),IT(M),DIR(N,M),SPD(N,M),M=1,NTOBS),N=1,44)
100   FORMAT(A3,8X,I4,2X,F4.0,F4.0)
      WRITE(LO,103)(STA(N),N=1,44)
103   FORMAT(18H1ORDER OF STATIONS/(1H ,A3))
19    READ( 5 ,102) RE,FNU,NT
102   FORMAT(2F5.0,I5)
      REWIND 4
```

```
C    INPUT STORM VECTOR IN DEGREES AND KNOTS,ANALYSIS TIME AND CALCULATE
C            COMPONENTS OF STORM VECTOR
21     READ( 5 ,101) SD,SS,NTIME,IDT
101    FORMAT(F4.0,F5.1,I5,1X,I6)
       CALL DISPLA(20H NOW WORKING AT TIME,NTIME)
       IF(NTIME.EQ.99999) GO TO 36
       ANG=SD/RAD
       SU=-SS*SIN(ANG)
       SV=-SS*COS(ANG)
C    CALCULATE COMPONENTS OF ACTUAL AND RELATIVE WIND FIELD IN KNOTS
       DO 22 N=1,44
       DO 22 M=1,NTOBS
       IF(DIR(N,M).NE.999.) GO TO 221
       U(N,M)=999.
       V(N,M)=999.
       GO TO 22
221    ANG=DIR(N,M)/RAD
       U(N,M)= -SPD(N,M)*SIN(ANG)
       V(N,M)= -SPD(N,M)*COS(ANG)
22     CONTINUE
       DU=SU*CT
       DV=SV*CT
C     CALCULATE DISPLACEMENTS (KM) OF NT OBSERVATIONS SURROUNDING MAPTIME
       DO 23 L=1,NT
       FJ=L-(NT/2 + 1)
       DX(L)=DU*FJ
23     DY(L)=DV*FJ
C     CALCULATE LOCATIONS INDEXES OF DATA TO BE ANALYZED
       DO 25 M=1,NTOBS
       IF(IT(M).NE.NTIME) GO TO 25
       J=M+NT/2
       DO 24 L=1,NT
24     KT(L)= J-L+1
       GO TO 26
25     CONTINUE
C     GENERATE TIME  DIFFERENCES BETWEEN OBS AND MAP TIME
26     DT(1)= 5*(NT/2)
       DO 27 L=2,NT
27     DT(L)=DT(L-1) - 5.
C     CALCULATE DISPLACEMENTS IN KM FROM NORMAN FOR  EACH OB
       DO 29 N=1,44
       DO 29 L=1,NT
       XL(N,L)=XS(N) + DX(L)
       YL(N,L)=YS(N) + DY(L)
C     CALCULATE GRID POINT NEAREST EACH OB
       XX=XL(N,L)/3.175
       YY=YL(N,L)/3.175
       I=(XX-FLOAT(IFIX(XX))) + XX
       J=(YY-FLOAT(IFIX(YY))) + YY
       I=27 + I
       J= 20-J
       IF(I.LT.1) I=1
       IF(I.GT.36) I=36
       IF(J.LT.1) J=1
       IF(J.GT.30) J=30
       IMIN(N,L)=I
29     JMIN(N,L)=J
```

```
      WRITE(LO,200)KK(1),IDT,NTIME,RE,FNU,SD,SS
200   FORMAT(1H1,A4,9H    ACTUAL,5X,4HDATE,I7,3X,4HTIME,I5,4H CST,5X,
     13HRE=,F5.0,2X,4HFNU=,F6.0,5X,12HSTORM VECTOR,F7.0,1H/,F4.1)
      CALL INTERP(U,5,1.,DGP)
      WRITE(LO,200)KK(2),IDT,NTIME,RE,FNU,SD,SS
      CALL INTERP(V,5,1.,SAVE)
      CALL DIV(DGP,SAVE,DEL)
      WRITE(LO,200)KK(5),IDT,NTIME,RE,FNU,SD,SS
      CALL CONTUR(50)
      CALL VORT(DGP,SAVE,DEL)
      WRITE(LO,200)KK(6),IDT,NTIME,RE,FNU,SD,SS
      CALL CONTUR(50)
      DO 32 J=1,20
      DO 32 I=1,24
32    MAP(I,J)=DGP(I,J)
      WRITE(LO,200)KK(3),IDT,NTIME,RE,FNU,SD,SS
      CALL CONTUR(5)
      DO 33  J=1,20
      DO 33  I=1,24
33    MAP(I,J)=SAVE(I,J)
      WRITE(LO,200)KK(4),IDT,NTIME,RE,FNU,SD,SS
      CALL CONTUR(30)
C     ACTUAL WIND FIELD ANALYZED TO THIS POINT
      WRITE(LO,250)KK(3),IDT,NTIME,RE,FNU,SD,SS,SU,SV
250   FORMAT(1H1,A4,9H RELATIVE,5X,4HDATE,I7,3X,4HTIME,I5,4H CST,5X,
     13HRE=,F5.0,2X,4HFNU=,F6.0,5X,12HSTORM VECTOR,F7.0,1H/,F4.1,
     23X,3HSU=,F5.1,3X,3HSV=,F5.1)
      DO 34 J=1,20
      DO 34 I=1,24
34    MAP(I,J)=SQRT(UR(I,J)*UR(I,J)+VR(I,J)*VR(I,J))
      CALL CONTUR(5)
      DO 35 J=1,20
      DO 35 I=1,24
35    MAP(I,J)=ADIR(UR(I,J),VR(I,J))
      WRITE(LO,250)KK(4),IDT,NTIME,RE,FNU,SD,SS,SU,SV
      CALL CONTUR(30)
      GO TO 21
36    CONTINUE
      CALL EXIT
      END


      FUNCTION ADIR(U,V)
600   IF(U)610,620,630
610   ADIR=90.-57.2958*ATAN(V/U)
      GO TO 640
630   ADIR=270.-57.2958*ATAN(V/U)
      GO TO 640
620   IF(V)650,660,670
650   ADIR=360.
      GO TO 640
660   ADIR=999.
      GO TO 640
670   ADIR=180.
640   RETURN
      END
```

```
      SUBROUTINE INTERP(P,INT,FACTOR,DGP)
      DIMENSION P(44,109),DIF(44,7),DGP(36,30),XGP(36),YGP(30)
      COMMON KT(07),DT(07),XL(44,07),YL(44,07),IMIN(44,07),
     1   JMIN(44,07),MAP(24,20),RE,FNU,SU,SV,UR(24,20),VR(24,20),NT,LO
      DATA XGP/-82.55,-79.375,-76.2,-73.025,-69.85,-66.675,-63.5,
     1-60.325,-57.15,-53.975,-50.8,-47.625,-44.45,-41.275,-38.1,-34.925,
     2-31.75,-28.575,-25.4,-22.225,-19.05,-15.875,-12.7,-9.525,-6.35,
     3-3.175,0.,3.175,6.35,9.525,12.7,15.875,19.05,22.225,25.4,28.575/
      DATA YGP/                    60.325,57.15,53.975,50.8,47.625,44.45,
     141.275,38.1,34.925,31.75,28.575,25.4,22.225,19.05,15.875,12.7,
     29.525,6.35,3.175,0.,-3.175,-6.35,-9.525,-12.7,-15.875,-19.05,
     3-22.225,-25.4,-28.575,-31.75/
      NREP=0
      A=RE
      B=FNU
      INT=INT
9     DO 14 J=1,30
      DO 14 I=1,36
      SUM1=0.
      SUM2=0.
      DO 12 N=1,44
      DO 12 L=1,NT
      K=KT(L)
      IF(P(N,K).EQ.999.) GO TO 12
      XX=XL(N,L)-XGP(I)
      YY=YL(N,L)-YGP(J)
      R2=XX*XX+YY*YY
      T2=DT(L)**2
      EWT=-R2/A - T2/B
      WT=EXP(EWT)
      IF(NREP.EQ.1) GO TO 10
      SUM1=SUM1+WT*P(N,K)
      GO TO 11
10    SUM1=SUM1+WT*DIF(N,L)
11    SUM2=SUM2+WT
12    CONTINUE
      IF(SUM2.EQ.0.) SUM2=1.
      IF(NREP.EQ.0) GO TO 13
      DGP(I,J)=DGP(I,J) + SUM1/SUM2
      GO TO 14
13    DGP(I,J)=SUM1/SUM2
14    CONTINUE
      IF(NREP.EQ.1) GO TO 17
      DO 16 N=1,44
      DO 16 L=1,NT
      K=KT(L)
      I=IMIN(N,L)
      J=JMIN(N,L)
16    DIF(N,L)=P(N,K)-DGP(I,J)
      NREP=1
      A=RE*0.5
      GO TO 9
17    DO 18 J=1,20
      DO 18 I=1,24
18    MAP(I,J)=DGP(I+6,J+5)*FACTOR + SIGN(0.5,DGP(I+6,J+5))
      CALL CONTUR(INT)
      RETURN
      END
```

```
      SUBROUTINE CONTUR(INT)
      DIMENSION KALP(17),LINE(131),LIN(24)
      COMMON KT(07),DT(07),XL(44,07),YL(44,07),IMIN(44,07),
     1  JMIN(44,07),MAP(24,20),RE,FNU,SU,SV,UR(24,20),VR(24,20),NT,LO
      DATA KALP/1H ,1HA,1H ,1HB,1H ,1HC,1H ,1HD,1H ,1HE,1H ,1HF,1H ,
     *       1HG,1H ,1HH,1H*/
      MIN=MAP(1,1)
      MARK=KALP(1)
      DO 101 J=1,20
      DO 101 I=1,24
      M=MAP(I,J)
      IF(M.GT.99999.OR.M.LT.-9999)M=99999
      IF(M.LT.MIN) MIN=M
101   CONTINUE
      IF(MIN.GE.0) GO TO 102
      MIN=(MIN/INT-1)*INT *10
      GO TO 104
102   MIN=(MIN/INT)*INT *10
104   WRITE(LO,201)(MAP(I,1),I=1,24)
201   FORMAT(/1H0,2415)
      INT10=INT*10
      DO 1 JR=2,20
      DO 2 JJ=1,2
      DO 3 L=1,24
3     LIN(L)=((MAP(L,JR)-MAP(L,JR-1))*JJ*10)/3+MAP(L,JR-1)*10
      K=1
      DO 4 I=1,23
      LINI=LIN(I)
      LINE(K)=LINI
      NDZ=LIN(I+1)-LINI
      DO 5 L=1,4
      K=K+1
5     LINE(K)=(NDZ*L)/5+LINI
      K=K+1
4     CONTINUE
      LINE(K)=LIN(24)
      ICOUNT=1
      M=4
      GO TO 1212
1313  ICOUNT=L+5
      M=4
1212  DO 6060 L=ICOUNT,116
      M=M+1
      K=M/5
      IF(K.EQ.1) GO TO 1010
1111  IDF=LINE(L)-MIN
      I=IDF/INT10
      IS=I-(I/16)*16+1
      LINE(L)=KALP(IS)
      GO TO 6060
1010  M=0
      IF(L.EQ.116) GO TO 1111
      NDZ=LINE(L)-LINE(L+5)
      IF(IABS(NDZ).LT.4*INT10) GO TO 1111
```

```
      LP1=L+1
      LP2=L+2
      LP3=L+3
      LP4=L+4
      LINE(L)=KALP(1)
      LINE(LP1)=KALP(1)
      LINE(LP2)=KALP(1)
      LINE(LP3)=KALP(1)
      LINE(LP4)=KALP(1)
      GO TO 1313
6060  CONTINUE
      IF(JR.EQ.16.AND.JJ.EQ.1) MARK=KALP(17)
      WRITE(LO,901)MARK,(LINE(L),L=1,116)
901   FORMAT(1H ,A1,3X,116A1)
      MARK=KALP(1)
2     CONTINUE
      WRITE(LO,900)(MAP(I,JR),I=1,24)
900   FORMAT(1H ,24I5)
1     CONTINUE
      DO 7 L=1,116
7     LINE(L)=KALP(1)
      LINE(101)=KALP(17)
      WRITE(LO,901)MARK,(LINE(L),L=1,116)
      RETURN
      END



      SUBROUTINE DIV(DGP,SAVE,DEL)
      DIMENSION DGP(36,30),SAVE(36,30)
      COMMON KT(07),DT(07),XL(44,07),YL(44,07),IMIN(44,07),
     1  JMIN(44,07),MAP(24,20),RE,FNU,SU,SV,UR(24,20),VR(24,20),NT,LO
      DO 30 J=1,20
      DO 30 I=1,24
      UR(I,J)=DGP(I+6,J+5)-SU
      VR(I,J)=SAVE(I+6,J+5)-SV
30    MAP(I,J)=DEL*(DGP(I+7,J+5)-DGP(I+5,J+5)+SAVE(I+6,J+4)-SAVE(I+6,J+6
     1))
      RETURN
      END



      SUBROUTINE VORT(DGP,SAVE,DEL)
      DIMENSION DGP(36,30),SAVE(36,30)
      COMMON KT(07),DT(07),XL(44,07),YL(44,07),IMIN(44,07),
     1  JMIN(44,07),MAP(24,20),RE,FNU,SU,SV,UR(24,20),VR(24,20),NT,LO
      DO 31 J=1,20
      DO 31 I=1,24
      MAP(I,J)=DEL*(SAVE(I+7,J+5)-SAVE(I+5,J+5)-DGP(I+6,J+4)+DGP(I+6,J+6
     1))
      DGP(I,J)=SQRT(SAVE(I+6,J+5)*SAVE(I+6,J+5)+DGP(I+6,J+5)*DGP(I+6,J+5
     1))
31    SAVE(I,J)=ADIR(DGP(I+6,J+5),SAVE(I+6,J+5))
      RETURN
      END
```

APPENDIX C

Upper Air Analysis Program

Bookkeeping functions in this program are considerably more complicated than those of the surface analysis program (appendix B). The irregular times of observation and drift of balloons in space necessitate the more elaborate treatment. The program calculates distributions of both wind and thermodynamic variables, whereas the surface program treated wind data only (other variables are analyzed in separate programs). The input data for this FORTRAN IV program are the NSSL rawinsonde archive tapes (see Barnes et al., 1971). Control parameters input from cards include:

IO	I index (in +x direction) of center grid point.
JO	J index (in -y direction) of center grid point.
NX	Total number of grid points in x direction.
NY	Total number of grid points in -y direction.
DEL	Mesh size (km).
XO	Location (km) of center point (at station WHT)
YO	from NSSL. Grid is rotated about this point such that x axis aligns along storm vector.
MS	Total number of soundings applicable to analysis.
STAR	Characteristic speed V* (m sec^{-1}) for along the wind weight enhancement. See (40).
RE	4k (see (19)).
FNU	4ν (see (19)).
Z	Analysis level (meters above mean sea level).
MXR	Mixing ratio contour interval (10 = 1 g kg^{-1}).
ZA	Height of data to which following confidence factors apply.
M	Station identification number.
L	Sounding number in this series.
A	Confidence factor for wind data.
B	Confidence factor for theormodynamic data.
SD	Storm direction (from).
SS	Storm speed (kts).
TIME	Reference map time.
IDT	Data.

In addition to the subroutines identified in appendix B, balloon positions are plotted in subroutine XYPLOT. This allows convenient checks between data and analyzed features.

```
C       PHASE 1 ANALYSIS FOR 1970 RAWINSONDE DATA REVISION G  JAN 1972
        DIMENSION ID(9,8),X(9,8),Y(9,8),TM(9,8),T(9,8),AM(9,8),WBPT(9,8),
       1   U(9,8),V(9,8),SR(9,8),DX(9,7),DR(9,8),XS(9),YS(9),DGP(35,19),
       2   SAVE(35,19),KK(11),UG(9,8),VG(9,8),TA(9,8),WA(9,8),AN(9,8)
        COMMON UR(25,17),VR(25,17),NEAR(9),DELT(9,8),XL(9,8),YL(9,8),
       1ILLCU9,8),JLLC(9,8),MAP(25,19),RE,FNU,SU,SV,STAR,XGP(35),YGP(19),
       2D(9,8),S(9,8),LSAVE(9),TEST,XO,YO,B,C,DEL,SD,RAD,RMS,BAR
        DATA XS/-45.5,-17.1,5.3,-44.0,-17.5,6.0,-47.4,-26.0,3.4/
        DATA YS/-15.0,-8.6,-8.9,10.7,16.9,19.0,32.0,45.4,47.3/
        DATA KS/2H1S/
        DATA KK/4HWBPT,4HTEMP,4H MXR,4H   U,4H   V,4H DIV,4HVORT,4H SPD,
       14H DIR,4H  XY,4HWIND/
        DXY=100000./12700.
        CT=1.853248/60.
        RAD=57.29578
        READ(5,1) IO,JO,NX,NY,DEL,XO,YO,MS
1       FORMAT(2I3,2I4,F6.3,2F7.1,I4)
        TEST=FLOAT(NX/2)*DEL
        READ(5,520) STAR,RE,FNU
520     FORMAT(3F10.0)
        XGP(1)=FLOAT(1-IO)*DEL
        YGP(1)=FLOAT(JO-1)*DEL
        DO 3 K=2,NX
3       XGP(K)=XGP(K-1)+DEL
        DO 4 K=2,NY
4       YGP(K)=YGP(K-1)-DEL
3000    DO 45 M=1,9
        DO 45 L=1,8
        ID(M,L)=0
        TA(M,L)=1.
        WA(M,L)=1.
        AN(M,L)=999.
        X(M,L)=999.
        Y(M,L)=999.
        S(M,L)=999.
        D(M,L)=999.
        T(M,L)=999.
        TM(M,L)=999.
        AM(M,L)=999.
        XL(M,L)=999.
        YL(M,L)=999.
        U(M,L)=999.
        V(M,L)=999.
        UG(M,L)=999.
        VG(M,L)=999.
        SR(M,L)=999.
        DR(M,L)=999.
        DELT(M,L)=999.
45      WBPT(M,L)=999.
        READ(5,6) Z,MXR
6       FORMAT(F6.0,I5)
        IF(Z.EQ.0.) GO TO 36
        REWIND 4
9       WRITE(6,801)
        NS=0
```

```
      DO 8 K=1,9
8     LSAVE(K)=0
5     READ(5,2) ZA,M,L,A,B
2     FORMAT(F5.0,2I2,2F4.1)
      IF(M.EQ.0) GO TO 1000
      IF(ZA.NE.Z) GO TO 5
      TA(M,L)=A
      WA(M,L)=B
      GO TO 5
1000  READ(4,76) KEY
76    FORMAT(A2)
      IF(EOF(4)) 5000,5001
5000  PRINT 5002, NS,KEY,SSS,ISN,Z
5002  FORMAT(I3,A2,A3,I5,F7.0)
      GO TO 36
5001  IF(KEY.NE.KS) GO TO 1000
      READU4,78)SSS,LDATE,LTIME,IRSN,HTS,SLAT,SLONG,IDD,ISN,ICN
78    FORMAT(1H ,A3,2X,2I6,I7,F5.0,F6.2,F7.2,3X,I2,I6,I7)
      IF(SSS.EQ.3HEDM.AND.LTIME.EQ.0127)GO TO 6932
      ICN=ICN/100
      IF(ICN.NE.12) GO TO 1000
      NS=NS+1
      M=IDD
      READ(4,300)
      READ(4,300)
      READ(4,85) MAX
85    FORMAT(8H MAX =   ,I3)
      READ(4,300)
300   FORMAT(1H ,19X)
      DO 86 N=1,MAX
      IF(N.EQ.111) READ(4,300)
      READ(4,303)H,P1,T1,TD1,AM1,SPD1,DIR1,U1,V1,X1,Y1,TM1
303   FORMAT(1H ,2F7.1,2F6.1,6X,F7.2,26X,F6.1,F6.0,2F6.1,15X,2F8.3,F7.2)
      IF(H.EQ.Z) GO TO 20
86    CONTINUE
      WRITE(6,304) Z,SSS,ISN,LTIME
304   FORMAT(21H0UNABLE TO FIND LEVEL,F7.0,9H DATA FOR,5X,A3,5X,
     16HASCENT,I5,5X,4HTIME,I6)
      GO TO 1000
20    L=LSAVE(M)+1
      LSAVE(M)=L
      IF(DIR1.NE.999.) GO TO 21
      SPD1=999.
      U1=999.
      V1=999.
      X1=0.
      Y1=0.
21    TLC=TD1-(0.001296*TD1+0.1963)*(T1-TD1)
      TLK=TLC+273.16
      TK=T1+273.16
      PD=P1*(1.-(TLK/TK)**3.5)
      P2=P1-PD
      PS=P2*P2
      P3=P2*PS
      B=-102.40678+0.29999*P2-(2.764E-4)*PS+9.9E-8*P3
```

```
      IF(TLC-B)401,402,402
401   A=-135.01805+0.33800929*P2-2.887E-4*PS+9.6E-8*P3
      WBPT(M,L)=10.+(TLC-A)*10./(B-A)
      GO TO 115
402   C=-56.5666+0.1973568*P2-1.705E-4 *PS+5.98E-8*P3
      WBPT(M,L)=20.+(TLC-B)*10./(C-B)
115   T(M,L)=T1
      AM(M,L)=AM1
      U(M,L)=U1
      V(M,L)=V1
      X(M,L)=X1
      Y(M,L)=Y1
      S(M,L)=SPD1
      D(M,L)=DIR1
      AN(M,L)=ISN
      LH=LTIME/100
      LM=LTIME - LH*100
      TM1=FLOAT(LM) + TM1
209   IF(TM1.LT.60.) GO TO 210
      LH=LH+1
      TM1=TM1-60.
      GO TO 209
210   TM1=FLOAT(LH)*100. + TM1
      IF(TM1.LT.0600.) TM1=TM1+2400.
      TM(M,L)=TM1
      ID(M,L)=M
      IF(NS.NE.MS) GO TO 1000
 6932 REWIND 4
C     IF DISPLACEMENT IS UNAVAILABLE OR NO CONFIDENCE, SEARCH FOR
C     CLOSEST OB FROM THIS STATION HAVING GOOD DISP AND SUBSTITUTE.
C     REDUCE CONFIDENCE PARAMETER FOR THERMO DATA BY 20 PER CENT.
      DO 113 M=1,9
      N=LSAVE(M)
      IF(N.EQ.0) GO TO 113
      DO 112 L=1,N
      IF(D(M,L).EQ.999..OR.WA(M,L).EQ.0.) GO TO 114
      GO TO 112
114   I=1
      K=1
      J=L
111   J=J+K
      IF(J.GT.N.OR.J.LT.1) GO TO 110
      IF(D(M,J).EQ.999..OR.WA(M,J).EQ.0.) GO TO 110
      X(M,L)=X(M,J)
      Y(M,L)=Y(M,J)
      TA(M,L)=0.8*TA(M,L)
      GO TO 112
110   K=-I*(IABS(K)+1)
      I=-I
      GO TO 111
112   CONTINUE
113   CONTINUE
2000  READ(5,7) SD,SS,TIME,IDT
7     FORMAT(F4.0,F5.1,F5.0,1X,I6)
```

```
      IF(TIME.EQ.99999.) GO TO 3000
      IF(TIME.LT.0600.) TIME=TIME+2400.
C     CONVERTS KNOTS TO KM/MIN
      SS=SS*CT
      ANG=(270.-SD)/RAD
      B=SIN(ANG)
      C=COS(ANG)
      PHI=SD/RAD
C     COMPONENTS OF STORM VECTOR IN M/SEC
      SU=-SS*SIN(PHI)*1000./60.
      SV=-SS*COS(PHI)*1000./60.
      DO 116 M=1,9
      N=LSAVE(M)-1
      IF(N.LE.0) GO TO 116
      DO 117 L=1,N
      IT1=TM(M,L)/100.
      IT2=TM(M,L+1)/100.
      HR=(IT2-IT1)*60
      FT1=IT1*100
      FT2=IT2*100
      DT      =TM(M,L+1)-FT2-TM(M,L)+FT1+HR
      DX(M,L)=-SS*DT
117   CONTINUE
116   CONTINUE
C     GENERATE ARRAY OF TIME DIFFERENCES IN MIN BETWEEN EACH OB AND MAP TI
      DO 118 M=1,9
      N=LSAVE(M)
      IF(N.EQ.0) GO TO 118
      DO 119 L=1,N
      IT1=TM(M,L)/100.
      IT2=TIME/100.
      HR=(IT2-IT1)*60
      FT1=IT1*100
      FT2=IT2*100
      DELT(M,L)=TM(M,L)+FT2-TIME-FT1-HR
      A=X(M,L)+XS(M)-XO
      TK=Y(M,L)+YS(M)-YO
      XL(M,L)=A*C + TK*B
      YL(M,L)=TK*C-A*B
119   CONTINUE
118   CONTINUE
C     FIND OB NEAREST MAP TIME AND USE THAT BALLOON DISPLACEMENT
C     AS THE ORIGIN FOR POSITIONING DATA LINE. (FIND THE L OF NEAREST OB)
      DO 18 M=1,9
      N=LSAVE(M)-1
      NEAR(M)=1
      IF(N) 17,18,70
70    DO 16 L=1,N
      TEST1=ABS(DELT(M,L))
      TEST2=ABS(DELT(M,L+1))
      IF(TEST1.GT.TEST2) NEAR(M)=L+1
16    CONTINUE
      GO TO 18
17    NEAR(M)=0
18    CONTINUE
```

```
C     CALCULATE DISPLACEMENT OF NEAREST OB IN TIME FROM MAP TIME
      DO 28 M=1,9
      L=NEAR(M)
      IF(L.EQ.0) GO TO 28
      DTX=-DELT(M,L)*SS
C     CALC DISPLACEMENT (KM) OF OBSERVATION FROM WHT IN GRID COORDINATES
      XL(M,L)=XL(M,L) + DTX
C     CALCULATE DISPLACEMENT OF EACH OTHER OB FROM NEAREST OB REF GRID
25    L=L-1
      IF(L.EQ.0) GO TO 26
      XL(M,L)=XL(M,L+1)-DX(M,L)
      GO TO 25
26    L=NEAR(M)
27    L=L+1
      IF(L.GT.LSAVE(M)) GO TO 28
      XL(M,L)=XL(M,L-1)+DX(M,L-1)
      GO TO 27
28    CONTINUE
C     DETERMINE I AND J AT LOWER LEFT CORNER OF GRID BOX CONTAINING OB
      DO 38 M=1,9
      N=LSAVE(M)
      IF(N.EQ.0) GO TO 38
      DO 37 L=1,N
      DO 12 J=2,19
      IF(YL(M,L).GT.YGP(J)) GO TO 13
12    CONTINUE
      J=J-1
13    DO 10 I=2,35
      IF(XL(M,L).LT.XGP(I)) GO TO 11
10    CONTINUE
      I=I-1
11    ILLC(M,L)=I-1
37    JLLC(M,L)=J
38    CONTINUE
      IF(TIME.GE.2400.) TIME=TIME-2400.
      NTIME=TIME
C     STORM SPEED CONVERTED TO MPS
      SS=SS*1000./60.
C     CALC RELATIVE WINDS AND CONVERT U,V COMPONENTS OF ACTUAL WIND TO
C     GRID COMPONENTS
      DO 52 M=1,9
      DO 52 L=1,8
      IF(D(M,L).EQ.999.) GO TO 52
      U1=U(M,L)-SU
      V1=V(M,L)-SV
      SR(M,L)=SQRT(U1*U1+V1*V1)
      DR(M,L)=ADIR(U1,V1)
      UG(M,L)=U(M,L)*C+V(M,L)*B
      VG(M,L)=V(M,L)*C-U(M,L)*B
52    CONTINUE
801   FORMAT(1H1,19X)
      B=0.
      BAR=9999.9
      RMS=9999.9
      WRITE(6,200)KK(1),IDT,NTIME,RE,FNU,STAR,SD,SS,Z,B,BAR,RMS
```

```
      DO 50 M=1,9
      WRITE(6,800) M,(AN(M,L),XL(M,L),L=1,8)
      WRITE(6,800) M,(DELT(M,L),YL(M,L),L=1,8)
      WRITE(6,800) M,(TM(M,L),WBPT(M,L),L=1,8)
50    WRITE(6,300)
800   FORMAT(1H ,I3,8(3X,F5.0,F7.1))
      WRITE(6,802)
802   FORMAT(1H ,15X,1H1,14X,1H2,14X,1H3,14X,1H4,14X,1H5,14X,1H6,14X,
     11H7,14X,1H8)
      WRITE(6,200) KK(11),IDT,NTIME,RE,FNU,STAR,SD,SS,Z,B,BAR,RMS
      DO 51 M=1,9
      WRITE(6,800)M,(TM(M,L),S(M,L),L=1,8)
      WRITE(6,800)M,(DELT(M,L),D(M,L),L=1,8)
51    WRITE(6,300)
      WRITE(6,802)
      WRITE(6,200) KK(11),IDT,NTIME,RE,FNU,STAR,SD,SS,Z,B,BAR,RMS
      DO 53 M=1,9
      WRITE(6,800) M,(TM(M,L),SR(M,L),L=1,8)
      WRITE(6,800) M,(DELT(M,L),DR(M,L),L=1,8)
      WRITE(6,300)
53    CONTINUE
      WRITE(6,802)
      WRITE(6,200) KK(10),IDT,NTIME,RE,FNU,STAR,SD,SS,Z,B,BAR,RMS
200   FORMAT(1H1,A4,5X,4HDATE,I7,3X, 4HTIME,I5,4H CST,5X,
     13HRE=,F5.0,2X,4HFNU=,F6.0,5X,5HSTAR=,F5.0,5X,12HSTORM VECTOR,F7.0,
     21H/,F4.1,10X,6HLEVEL=,F6.0,2H M/42X,4HNO.=,F4.0,2X,4HBAR=,F7.1,4X,
     34HRMS=,F7.1)
      CALL XYPLOT(AN)
      CALL INTERP(WBPT,10,10.,DGP,1.0,90.,TA)
      WRITE(6,200)KK(1),IDT,NTIME,RE,FNU,STAR,SD,SS,Z,B,BAR,RMS
      CALL CONTUR(10,61,10,17)
      CALL INTERP(T,10,10.,DGP,0.5,90.,TA)
      WRITE(6,200)KK(2),IDT,NTIME,RE,FNU,STAR,SD,SS,Z,B,BAR,RMS
      CALL CONTUR(10,61,10,17)
      CALL INTERP(AM,MXR,10.,DGP,0.5,90.,TA)
      WRITE(6,200)KK(3),IDT,NTIME,RE,FNU,STAR,SD,SS,Z,B,BAR,RMS
      CALL CONTUR(MXR,61,10,17)
      CALL INTERP(UG,50,10.,DGP,1.0,90.,WA)
      WRITE(6,200)KK(4),IDT,NTIME,RE,FNU,STAR,SD,SS,Z,B,BAR,RMS
      CALL CONTUR(50,61,10,17)
      CALL INTERP(VG,50,10.,SAVE,1.0,90.,WA)
      WRITE(6,200)KK(5),IDT,NTIME,RE,FNU,STAR,SD,SS,Z,B,BAR,RMS
      CALL CONTUR(50,61,10,17)
      CALL DIV(DGP,SAVE,DXY,SS)
      B=0.
      BAR=9999.9
      RMS=9999.9
      WRITE(6,200)KK(6),IDT,NTIME,RE,FNU,STAR,SD,SS,Z,B,BAR,RMS
      CALL CONTUR(50,61,10,17)
      CALL VORT(DGP,SAVE,DXY)
      WRITE(6,200)KK(7),IDT,NTIME,RE,FNU,STAR,SD,SS,Z,B,BAR,RMS
      CALL CONTUR(50,61,10,17)
```

```
      DO 32 J=1,17
      DO 32 I=1,25
      MAP(I,J)=DGP(I,J)*10.
   32 CONTINUE
      WRITE(6,200)KK(8),IDT,NTIME,RE,FNU,STAR,SD,SS,Z,B,BAR,RMS
      CALL CONTUR(50,61,10,17)
      DO 33 J=1,17
      DO 33 I=1,25
      MAP(I,J)=SAVE(I,J)
   33 CONTINUE
      WRITE(6,200)KK(9),IDT,NTIME,RE,FNU,STAR,SD,SS,Z,B,BAR,RMS
      CALL CONTUR( 30,61,10,17)
      DO 34 J=1,17
      DO 34 I=1,25
      MAP(I,J)=SQRT(UR(I,J)*UR(I,J)+VR(I,J)*VR(I,J))*10.
   34 CONTINUE
      WRITE(6,200)KK(8),IDT,NTIME,RE,FNU,STAR,SD,SS,Z,B,BAR,RMS
      CALL CONTUR(50,61,10,17)
      DO 35 J=1,17
      DO 35 I=1,25
      MAP(I,J)=ADIR(UR(I,J),VR(I,J))
   35 CONTINUE
      WRITE(6,200)KK(9),IDT,NTIME,RE,FNU,STAR,SD,SS,Z,B,BAR,RMS
      CALL CONTUR( 30,61,10,17)
      GO TO 2000
36    REWIND 4
      CALL EXIT
      END
```

```
      FUNCTION ADIR(U,V)
  600 IF(U)610,620,630
  610 ADIR=90.-57.2958*ATAN(V/U)
      GO TO 640
  630 ADIR=270.-57.2958*ATAN(V/U)
      GO TO 640
  620 IF(V)650,660,670
  650 ADIR=360.
      GO TO 640
  660 ADIR=999.
      GO TO 640
  670 ADIR=180.
  640 RETURN
      END
```

```
      SUBROUTINE INTERP(P,INT,FACTOR,DGP,DF,TL,ALPHA)
      DIMENSION P(9,8),DIF(09,08),DGP(35,19),ALPHA(9,8)
      COMMON UR(25,17),VR(25,17),NEAR(9),DELT(9,8),XL(9,8),YL(9,8),
     1ILLC(9,8),JLLC(9,8),MAP(25,19),RE,FNU,SU,SV,STAR,XGP(35),YGP(19),
     2D(9,8),S(9,8),LSAVE(9),TEST,XO,YO,B,C,DEL,SD,RAD,RMS,BAR
      ANG=270.-SD
      TSTS=7.*DEL
      NREP=0
      A=RE
      BB=FNU
      INT=INT
   45 DO 31 J=1,19
      DO 31 I=1,35
      SUM1=0.
      SUM2=0.
      DO 30 M=1,9
      N=LSAVE(M)
      IF(N.EQ.0) GO TO 30
      DO 29 L=1,N
      IF(P(M,L).EQ.999.) GO TO 29
      IF(ABS(XL(M,L)).GT.TEST) GO TO 29
      XX=XL(M,L)-XGP(I)
      YY=YL(M,L)-YGP(J)
      R2=XX*XX+YY*YY
      PHI=ADIR(XX,YY)
      IF(PHI.EQ.999.) PHI=D(M,L)+ANG
      RHO=(D(M,L)+ANG-PHI)/RAD
      E=COS(RHO)
      BETA=S(M,L)/STAR
      FK= A*(1.+BETA*E*E)
      T2=DELT(M,L)**2
      EWT=-R2/FK-T2/BB
      WT=ALPHA(M,L)*EXP(EWT)
      IF(NREP.GE.1) GO TO 50
      SUM1=SUM1+WT*  P(M,L)
      GO TO 51
   50 SUM1=SUM1+WT*DIF(M,L)
   51 SUM2=SUM2+WT
   29 CONTINUE
   30 CONTINUE
      IF(SUM2.EQ.0.) SUM2=1.
      IF(NREP.EQ.0) GO TO 41
      DGP(I,J)=DGP(I,J)+SUM1/SUM2
      GO TO 31
   41 DGP(I,J)=SUM1/SUM2
   31 CONTINUE
      DO 40 M=1,9
      N=LSAVE(M)
      IF(N.EQ.0) GO TO 40
      DO 39 L=1,N
      IF(P(M,L).EQ.999.) GO TO 39
      IF(ABS(XL(M,L)).GT.TEST) GO TO 39
      I=ILLC(M,L)
      J=JLLC(M,L)
      R=(XL(M,L)-XGP(I))/DEL
      Q=(YL(M,L)-YGP(J))/DEL
```

```
      OMR=1.-R
      OMQ=1.-Q
      DIF(M,L)=P(M,L)-(OMR*OMQ*DGP(I,J)+R*OMQ*DGP(I+1,J)+Q*OMR*
     1            DGP(I,J-1)+R*Q*DGP(I+1,J-1))
39    CONTINUE
40    CONTINUE
      NREP=NREP + 1
      A=A*0.343
      IF(NREP.LT.2) GO TO 45
      WRITE(6,48)
48    FORMAT(1H1,19X)
      B=0.
      SUM1=0.
      SUM2=0.
      DO 46 M=1,9
      N=LSAVE(M)
      IF(N.EQ.0) GO TO 46
      DO 47 L=1,N
      IF(P(M,L).EQ.999.) GO TO 47
      IF(ABS(XL(M,L)).GT.TSTS) GO TO 47
      IF(ALPHA(M,L).EQ.0.) GO TO 47
44    FORMAT(30H FOLLOWING ANALYSIS NOT WITHIN,F4.1,2X,10HAT STATION,
     1I3,2X,4HTIME,I3,5X,10HPARAMETER=,F10.3,3X,4HDIF=,F10.3,
     23X,5HDELT=,F7.0)
      E=DIF(M,L)
      WT=DELT(M,L)
      B=B+1.
      SUM1=SUM1+E
      SUM2=SUM2+E*E
      IF(ABS(E).GT.DF.AND.ABS(WT).LT.TL)WRITE(6,44)DF,M,L,P(M,L),E,WT
47    CONTINUE
46    CONTINUE
      BAR=SUM1/B
      RMS=SQRT(SUM2/B-(BAR*BAR))
      DO 18 J=1,17
      DO 18 I=1,25
18    MAP(I,J)=DGP(I+5,J+1)*FACTOR + SIGN(0.5,DGP(I+5,J+1))
      RETURN
      END
```

```
      SUBROUTINE CONTUR(INT,NCOL,NROW,NL)
      DIMENSION KALP(17),LINE(131),LIN(25)
      COMMON UR(25,17),VR(25,17),NEAR(9),DELT(9,8),XL(9,8),YL(9,8),
     1ILLC(9,8),JLLC(9,8),MAP(25,19),RE,FNU,SU,SV,STAR,XGP(35),YGP(19),
     2D(9,8),S(9,8),LSAVE(9),TEST,XO,YO,B,C,DEL,SD,RAD,RMS,BAR
      DATA KALP/1H ,1HA,1H ,1HB,1H ,1HC,1H ,1HD,1H ,1HE,1H ,1HF,1H ,
     *     1HG,1H ,1HH,1H*/
      MIN=MAP(1,1)
      MARK=KALP(1)
      DO 101 J=1,NL
      DO 101 I=1,25
      M=MAP(I,J)
      IF(M.GT.99999.OR.M.LT.-9999)M=99999
      IF(M.LT.MIN) MIN=M
101   CONTINUE
      IF(MIN.GE.0) GO TO 102
      MIN=(MIN/INT-1)*INT *10
      GO TO 104
102   MIN=(MIN/INT)*INT *10
104   WRITE(6,201)(MAP(I,1),I=1,25)
201   FORMAT(/1H0,25I5)
      INT10=INT*10
      DO 1 JR=2,NL
      DO 2 JJ=1,2
      DO 3 L=1,25
3     LIN(L)=((MAP(L,JR)-MAP(L,JR-1))*JJ*10)/3+MAP(L,JR-1)*10
      K=1
      DO 4 I=1,24
      LINI=LIN(I)
      LINE(K)=LINI
      NDZ=LIN(I+1)-LINI
      DO 5 L=1,4
      K=K+1
5     LINE(K)=(NDZ*L)/5+LINI
      K=K+1
4     CONTINUE
      LINE(K)=LIN(25)
      DO 6 L=1,121
      IDF=LINE(L)-MIN
      I=IDF/INT10
      IS=I-(I/16)*16+1
6     LINE(L)=KALP(IS)
      IF(JR.EQ.NROW.AND.JJ.EQ.1) MARK=KALP(17)
      WRITE(6,901) MARK,(LINE(L),L=1,121)
901   FORMAT(1H ,A1,3X,121A1)
      MARK=KALP(1)
2     CONTINUE
      WRITE(6,900)(MAP(I,JR),I=1,25)
900   FORMAT(1H ,25I5)
1     CONTINUE
      DO 7 L=1,121
7     LINE(L)=KALP(1)
      LINE(NCOL)=KALP(17)
      WRITE(6,901) MARK,(LINE(L),L=1,121)
      RETURN
      END
```

```
      SUBROUTINE XYPLOT(AN)
      DIMENSION KALP(12),LINE(130),IX(9,8),IY(9,8)
      DIMENSION AN(9,8)
      COMMON UR(25,17),VR(25,17),NEAR(9),DELT(9,8),XL(9,8),YL(9,8),
     1ILLCU9,8),JLLC(9,8),MAP(25,19),RE,FNU,SU,SV,STAR,XGP(35),YGP(19),
     2D(9,8),S(9,8),LSAVE(9),TEST,XO,YO,B,C,DEL,SD,RAD,RMS,BAR
      DATA KALP/1H1,1H2,1H3,1H4,1H5,1H6,1H7,1H8,1H9,1H*,1H ,1H./
      WRITE(6,902)
902   FORMAT(/1H0,19X)
      DO 10 M=1,9
      DO 10 L=1,8
      X=XL(M,L)/1.270 + 65.
      IX(M,L)=(X-FLOAT(IFIX(X))) + X
      Y=YL(M,L)/2.117
      IY(M,L)=(Y-FLOAT(IFIX(Y))) + Y
      IY(M,L)=25-IY(M,L)
10    CONTINUE
      DO 6 IR=1,49
      DO 3 L=1,130
3     LINE(L)=KALP(11)
      IF(IR.NE.25) GO TO 14
      DO 18 K=1,5
      KP=K+125
      LINE(K)=KALP(12)
18    LINE(KP)=KALP(12)
      LINE(65)=KALP(12)
14    DO 5 M=1,9
      DO 4 L=1,8
      IF(IR.NE.IY(M,L)) GO TO 4
      K=IX(M,L)
      IF(K.LT.4.OR.K.GT.130) GO TO 4
      KM1=K-1
      KM2=K-2
      KM3=K-3
      IAN=AN(M,L)
      IAT=IAN/10
      IAU=IAN-IAT*10
      LINE(KM3)=KALP(M)
      LINE(KM2)=KALP(IAT)
      LINE(KM1)=KALP(IAU)
      LINE(K)=KALP(10)
4     CONTINUE
5     CONTINUE
      WRITE(6,901) LINE
901   FORMAT(1H ,130A1,1X)
6     CONTINUE
      DO 7 L=1,130
7     LINE(L)=KALP(11)
      LINE(65)=KALP(12)
      WRITE(6,901) LINE
      RETURN
      END
```

P ≠ 0
2 6
8 2
2 7
7 1

```
      SUBROUTINE DIV(DGP,SAVE,DXY,SS)
      DIMENSION DGP(35,19),SAVE(35,19)
      COMMON UR(25,17),VR(25,17),NEAR(9),DELT(9,8),XL(9,8),YL(9,8),
     1ILLC(9,8),JLLC(9,8),MAP(25,19),RE,FNU,SU,SV,STAR,XGP(35),YGP(19),
     2D(9,8),S(9,8),LSAVE(9),TEST,XO,YO,B,C,DEL,SD,RAD,RMS,BAR
      DO 30 J=1,17
      DO 30 I=1,25
      UR(I,J)=DGP(I+5,J+1)-SS
      VR(I,J)=SAVE(I+5,J+1)
30    MAP(I,J)=DXY*(DGP(I+6,J+1)-DGP(I+4,J+1)+SAVE(I+5,J)-SAVE(I+5,J+2))
      RETURN
      END



      SUBROUTINE VORT(DGP,SAVE,DXY)
      DIMENSION DGP(35,19),SAVE(35,19)
      COMMON UR(25,17),VR(25,17),NEAR(9),DELT(9,8),XL(9,8),YL(9,8),
     1ILLC(9,8),JLLC(9,8),MAP(25,19),RE,FNU,SU,SV,STAR,XGP(35),YGP(19),
     2D(9,8),S(9,8),LSAVE(9),TEST,XO,YO,B,C,DEL,SD,RAD,RMS,BAR
      DO 31 J=1,17
      DO 31 I=1,25
      MAP(I,J)=DXY*(SAVE(I+6,J+1)-SAVE(I+4,J+1)-DGP(I+5,J)+DGP(I+5,J+2))
      DGP(I,J)=SQRT(SAVE(I+5,J+1)*SAVE(I+5,J+1)+DGP(I+5,J+1)*
     1DGP(I+5,J+1))
31    SAVE(I,J)=ADIR(DGP(I+5,J+1),SAVE(I+5,J+1))
      RETURN
      END
```


☆ U.S. GOVERNMENT PRINTING OFFICE: 1973 — 784-211 / 1134 REGION NO. 8